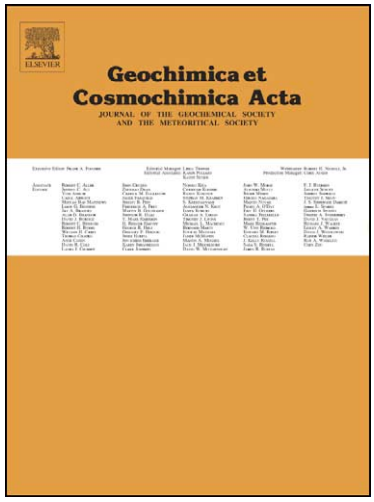

Arsenic incorporation into authigenic pyrite, Bengal Basin sediment, Bangladesh

Heather A. Lowers, George N. Breit, Andrea L. Foster, John Whitney, James Yount, Md. Nehal Uddin, Ad. Atual Muneem

PII: S0016-7037(07)00154-8
DOI: 10.1016/j.gca.2007.03.022
Reference: GCA 5156

To appear in: *Geochimica et Cosmochimica Acta*

Received Date: 11 October 2006
Accepted Date: 22 March 2007

Please cite this article as: Lowers, H.A., Breit, G.N., Foster, A.L., Whitney, J., Yount, J., Uddin, M.N., Muneem, A.A., Arsenic incorporation into authigenic pyrite, Bengal Basin sediment, Bangladesh, *Geochimica et Cosmochimica Acta* (2007), doi: 10.1016/j.gca.2007.03.022

Arsenic incorporation into authigenic pyrite, Bengal Basin sediment, Bangladesh

Heather A. Lowers[a,*], George N. Breit[a], Andrea L. Foster[b], John Whitney[c], James Yount[c], Md. Nehal Uddin[d] and Ad. Atual Muneem[d]

[a]*U.S. Geological Survey, MS 973, Denver, Colorado, U.S.A*
[b]*U.S. Geological Survey, MS 901, Menlo Park, California, U.S.A*
[c]*U.S. Geological Survey, MS 980, Denver, Colorado, U.S.A*
[d]*Geological Survey of Bangladesh, Segenbagicha, Dhaka, Bangladesh*

*Corresponding author. Tel.: 1-303-236-1184; fax: 1-303-236-3187; *email address*: hlowers@usgs.gov

Originally Submitted October 13, 2006
Accepted pending revision December 14, 2006
Resubmitted March 16, 2007

Abstract - Sediment from two deep boreholes (~400 m) approximately 90 km apart in southern Bangladesh was analyzed by x-ray absorption spectroscopy (XAS), total chemical analyses, chemical extractions, and electron probe microanalysis to establish the importance of authigenic pyrite as a sink for arsenic in the Bengal Basin. Authigenic framboidal and massive pyrite (median values 1500 and 3200 ppm As, respectively), is the principal arsenic residence in sediment from both boreholes. Although pyrite is dominant, ferric oxyhydroxides and secondary iron phases contain a large fraction of the sediment–bound arsenic between approximately 20 and 100 m, which is the depth range of wells containing the greatest amount of dissolved arsenic. The lack of pyrite in this interval is attributed to rapid sediment deposition and a low sulfur flux from riverine and atmospheric sources. The ability of deeper aquifers (>150 m) to produce ground water with low dissolved arsenic in southern Bangladesh reflects adequate sulfur supplies and sufficient time to redistribute the arsenic into pyrite during diagenesis.

1. INTRODUCTION

Arsenic substitution into early diagenetic pyrite and acid-volatile sulfide (AVS) is commonly proposed as a mechanism to account for removal of dissolved arsenic from pore water in marine and fresh water sediment (Farmer and Lovell, 1986; Huerta-Diaz and Morse, 1992; Sullivan and Aller, 1996;

Hideki and Yoshihisa, 1997; Saunders et al., 1997; Huerta-Diaz et al., 1998; Pirrie et al., 1999; Mucci et al., 2000; Sternbeck et al., 2000; O'Day et al., 2004; Saunders et al., 2005b; Southam and Saunders, 2005; Wilkin and Ford, 2006). Arsenic assimilation into forming sulfides commonly occurs as sediment is buried below the suboxic and sulfidic redox boundary. Masuda et al. (2005) observed arsenic-bearing oxides in shallow intertidal sediment off the coast of Japan and arsenic-bearing sulfides deeper in the sediment column. Sullivan and Aller (1996) report that arsenate in shallow Amazon shelf sediments is chemically reduced during burial, released to solution and removed from pore waters with increasing depth. Similarly, Moore et al. (1988) determined that arsenic bound to iron oxyhydroxides was redistributed into sulfide in reservoir sediment on the Clark Fork River, Montana.

The arsenic contamination in south and southeast Asia is attributed to redox changes, paleogeography, and tectonic setting whereby uplifted bedrock containing arsenic-rich minerals is weathered, rapidly eroded, and deposited in alluvial basins (Acharyya et al., 2000; Saunders et al., 2005a). The generally accepted model for high levels of dissolved arsenic proposes that arsenic released during weathering is absorbed onto neoformed ferric oxyhydroxides. During burial, bacteria use available organic matter to reductively dissolve the ferric oxyhydroxide grain coatings and release the arsenic to solution (Nickson et al., 2000; BGS and DPHE, 2001; Berg et al., 2001; Harvey et al., 2002; Islam et al., 2004; van Geen et al., 2004; Islam et al., 2005). Arsenic release by in situ oxidation of sulfide minerals in response to lowering water levels has been proposed but largely dismissed because of the lack of correlation of arsenic with dissolved sulfate (Acharyya, 2002). Independent of origin, the fate of dissolved arsenic in ground water is incompletely known. Arsenic-rich ground water either directly discharges into the Bay of Bengal or as base flow into rivers, which results in eventual flushing of labile arsenic from the aquifers. Alternatively, arsenic may be retained in the sediment in authigenic iron sulfide minerals. Both flushing and trapping of arsenic in sulfides would support the use of 'deeper' aquifers as a source of safer drinking water but risk evaluation would be markedly different depending on the relative importance of these two processes.

Although iron sulfide has been recognized as a constituent of the sediment in the Bengal Basin (Chatterjee et al., 1995; Nickson et al., 2000; BGS and DPHE, 2001; Acharyya, 2002; Stuben et al., 2003; Akai, 2004; McArthur et al., 2004; Swartz, 2004; Polizzotto et al., 2005; Ravenscroft et al., 2005), its relative importance and relation to the extensive arsenic-contaminated ground water in south and southeast Asia has not been fully evaluated. This study presents new information on the vertical variations in the abundance and morphology of iron sulfide, its arsenic content, sulfur isotope composition, and factors controlling its formation in shallow and deep sediment in southern Bangladesh.

1.1. Setting

The sediment underlying the villages of Rajoir and Srirampur in Bangladesh (Fig. 1) were selected to evaluate the ability of deeper (>150 m) aquifers to provide safe drinking water. The town of Rajoir (N 23.206 E 90.049), in the Rajoir upazila, Madaripur district, is 30 km south of the Padma River and 50 km west of the Meghna River. It is located on the lower Ganges floodplain and is typical of As-contaminated areas located on regularly flooded and actively aggrading floodplains. According to results presented by the National Arsenic Mitigation Information Center (NAMIC), approximately 71% of the 1340 wells tested within 3 km of the town of Rajoir exceed the Bangladesh drinking water standard of 50 ?g/L; similar frequency of high dissolved arsenic is reported for the greater Rajoir upazila (75% of 13,000 wells) (www.bwspp.org/photo_albam.html#screening%20Resulat). Srirampur (N 23.339; E 90.922) is a village in Kachua upazila, Chandphur district, 30 km east of the Meghna River. It is located on the lower delta and is part of the extensive flood basin considered part of the Meghna Estuary. The Srirampur borehole was located on alluvium whose surface is above normal levels of flooding, but may be inundated during an unusually large flood. Wells near Srirampur typically contain >50 ?g/L dissolved arsenic (99% of 3300 wells tested), which is similar to the 98% reported for the nearly 18,000 wells tested in the Kachua upazila (www.bwspp.org/photo_albam.html#screening%20Resulat). The high proportion of contaminated wells highlights the critical need for alternative supplies of drinking water in both areas.

As indicated by Ravenscroft et al. (2005), the stratigraphy of the Bengal Basin is poorly described. High Himalayan crystalline rocks have been the dominant source of sediment to the Bengal Basin since the Miocene. The thickness of sediment sampled for this study (450 m) is inferred to have been deposited mainly in the Quaternary, though Pliocene deposits may be present. The sediment sampled likely was deposited in a range of environments evident in the modern Bengal Basin. Fluvial channel, flood plain, estuarine, and deltaic deposits are stacked vertically and transition laterally. The complex spatial variability is attributed to changes in sea level, glaciation, tectonics and shifting river courses. Differences in the physical and chemical conditions of each of the depositional settings have been proposed to explain the kilometer-scale spatial heterogeneity of dissolved arsenic concentrations (Van Geen et al., 2003; 2006; McArthur et al., 2004).

2. METHODS

2.1. Sampling

Sediment samples were collected from active sand bars in the Meghna and Padma rivers; from 4 hand-dug excavations <5 m deep; and from cored intervals of two boreholes drilled to depths up to 450 m during 2003 and 2004 at Rajoir and Srirampur (Fig. 1). Sand bars were sampled using local watercraft. Shallow excavations included in this study were sampled where encountered during fieldwork within 5 km of the borehole locations.

Procedures used during sediment collection and chemical analyses are summarized below and presented in greater detail in Breit et al. (2006; 2007). Selected depth intervals of borehole sediment were recovered using a Shelby tube or split-spoon sampler. Bulk samples of shallow and borehole sediment were stored in plastic bags and air-dried. Subsamples were collected by inserting a detipped syringe into the core barrel to extract sediment prior to contact with air and transferring the sediment into a glass vial purged with flowing argon gas. The vials were promptly closed, flushed with additional argon through the septa, sealed with electrical tape, frozen in the field, and stored in a freezer (approximately -20° C) until shipment to the United States for analysis. The samples thawed during transport (~1 week) but upon

arrival were purged with high-purity nitrogen and refrozen. Because of the sampling method, results of the analyses of the preserved samples do not correspond directly to the bulk sample analyses.

2.2. Chemical analyses

Chemical composition of the sediment was determined by bulk analysis and chemical extractions. Chemical composition of the 115 bulk, air-dried sediment samples was determined by combustion, inductively-coupled plasma-atomic emission spectrometry, energy dispersive x-ray fluorescence, and hydride generation atomic absorption spectrophotometry (HGAAS) using methods described in Taggart et al. (2002). Results of the chemical and mineralogical analyses of the Srirampur and Rajoir borehole samples are presented in Breit et al. (2006) and (2007), respectively. Total sulfur concentrations were corrected for barite contamination from drilling mud in samples collected below 230 m at Srirampur and Rajoir as described by Breit et al. (2006; 2007).

Chemical extractions used to determine the abundance of iron species and sulfide forms are described in detail in Breit et al. (2006; 2007). Sequential iron extractions followed the general method of Heron and Christensen (1995) with the addition of an oxidative treatment to dissolve sulfide phases. Acid-soluble phases were extracted by treating 2 to 4 grams of 82 sediment samples from Rajoir and Srirampur with 40 mL of 0.5 N HCl in a sealed amber glass vial purged with high-purity nitrogen. Vials were shaken intermittently and stored in the dark for 24 hours. Solutions were withdrawn with a syringe, filtered through a 0.2 ?m filter and analyzed immediately with orthophenanthroline (Clesceri et al., 1998) to measure ferrous and total dissolved iron. Wilkin and Ford (2002) described the precipitation of arsenic sulfides as a likely result of extracting arsenic from sulfidic sediment using HCl. Evaluation of the content of AVS sulfide and arsenic extracted by 0.5 N HCl determined that reprecipitation is likely for only two samples from the Srirampur borehole and one from Rajoir (Breit et al., 2006; 2007). Srirampur sediment remaining after the 0.5 N HCl extraction was thoroughly rinsed with deionized water, air-dried and reacted for 24 hours with a solution of 0.008 M $TiCl_3$ and 0.05 M EDTA at pH 6.5 to dissolve

crystalline ferric oxides in a 50 mL serum vial purged with nitrogen. A mechanically split 0.5 gram fraction of the solid residue of the $TiCl_3$-EDTA extraction was treated with warm 20% hydrogen peroxide in 2 N HCl to dissolve sulfide phases. HGAAS and hydride generation atomic fluorescence spectroscopy was used to determine arsenic concentrations in extraction solutions.

Acid-volatile sulfide (AVS), acid-soluble sulfate and Cr^{2+} reducible sulfide (pyrite) were extracted from 28 samples with relatively high bulk-sulfur contents using the procedures of Tuttle et al. (1986) as modified by Rice et al. (1993). Samples first were treated with 6 N HCl amended with stannous chloride to recover AVS (FeS and greigite) and acid-soluble sulfate. The AVS residue was mixed with a solution of 4 N HCl and 1 M $CrCl_2$ to extract Cr^{2+} reducible sulfide (pyrite). Sulfide was precipitated as Ag_2S and sulfate as $BaSO_4$ for gravimetric measurement of sulfur forms and isotope analyses. The sulfur isotope composition of fertilizer and barite additive to drilling mud were also determined by dissolution and precipitation as $BaSO_4$. Sulfur isotope analyses followed the procedures of Kester et al. (2001).

2.3. X-ray absorption fine structure spectroscopy (XAFS)

Seven borehole samples for bulk XAFS analyses were kept frozen in inert-gas purged, sealed amber vials until shortly before analysis at the beamline (approximate holding time: 1-2 hours). Each sample was transferred into an anaerobic chamber for processing and loading. Sediments were ground (coarser material) or mixed in a mortar and pestle prior to loading into a 3 mm thick Teflon cell sealed with Mylar tape and placed onto an aluminum holder. The loaded sample was removed from the chamber, immediately dipped into liquid nitrogen, and kept frozen until analysis. Two subsamples from the Srirampur borehole (SH1-4, 39 m and SH1-36, 324 m) were prepared for microbeam XAS as described in Walker et al. (2005). A subset of the model compounds described below was analyzed as powders placed in glass capillaries or as single grains attached to Mylar tape for data calibration and comparison of resolution differences between beamlines.

Mineral model compounds were diluted and prepared for bulk and microXAFS analysis as previously described (Foster et al., 1998b). Arsenite ($As^{III}O_3$) and arsenate ($As^{V}O_4$) coprecipitates in

vivianite ($Fe_3(PO_4)_2 \cdot 8H_2O$) and siderite ($FeCO_3$), and adsorption samples on hydrous ferric oxide (HFO) were prepared in an anaerobic chamber (3% H_2/97%N_2) using oxygen-free solutions. Vivianite co-precipitates were protected from light to prevent oxidation. All ferrous mineral-arsenic coprecipitates were frozen immediately after synthesis and analyzed at low temperature to preclude ferrous iron oxidation. Co-precipitates of arsenic oxyanions in hydrous aluminum oxide (HAO) were prepared as described in Foster (1999).

Arsenic K-edge XAFS spectra of bulk samples were collected at the Stanford Synchrotron Radiation Laboratory (SSRL; ring conditions: 3 GeV and 50-90 mA) on beamline 11-2 over varying energy ranges (11,635-12,900 eV for high concentration model compounds and 11635-11920 eV for low-concentration borehole sediment) using a Si(220) monochromator and a 13- or 30-element germanium detector (Foster et al., 1998a). XAFS spectra of borehole samples and oxygen-sensitive model compounds (e.g. arsenite sorption samples) were collected at 10 K using a liquid helium-cooled cryostat. A comparison of spectra collected at ambient and low temperature revealed no difference in spectral line shape over the energy range used in this analysis.

Spatially-resolved XAFS (microXAFS) spectra and spatially-resolved X-ray fluorescence (microXRF) maps were collected under ambient conditions on beamline 10.3.2 at the Advanced Light Source (Berkeley, CA). MicroXAFS spectra of model compounds and samples were collected over the energy range 11,767-12167 eV. The X-ray beam ranged in size from 16 x 7 ?m to 5 x 5 ?m under operating conditions described in Marcus et al. (2004). The pixel size ranged from 9 x 9 ?m to 3 x 3 ?m, scan speeds ranged from 90 – 30 ?m/sec, and the dwell time was 100 milliseconds.

The method of XAFS data analysis was similar to that used in recent studies (Slowey et al., 2005). Data averaging (bulk XAFS spectra), data reduction (all spectra), and least squares fitting (all spectra) were accomplished using SixPACK (Webb, 2002); microXAFS spectra were averaged using "EXAFS editor.exe" and microXRF maps were viewed and interpreted using "XY display with mask.exe" developed by M. Marcus (ALS). Quantitative analysis of the identity and abundance of arsenic

species was ascertained by linear combination least-squares fits of model spectra representing arsenic in a variety of coordination environments to x-ray absoption near edge structure (XANES) spectra (for bulk sediments with low arsenic) or extended XANES spectra (for microbeam spots with higher arsenic). The accuracy of the fit procedure is approximately 10% (Foster et al., 1998a), but may be lower based on the signal-to-noise ratio of the analyzed spectrum. The operational detection limit of minor As species in bulk As K-edge XANES spectra is approximately 8% (Foster et al., 1998a). Details of the procedures used for spectral fits are given in electronic annex (EA) Appendix 1.

2.4. Electron microscopy methods

Twenty epoxy impregnated grain mounts were prepared for examination and analysis of sulfide mineral grains using a scanning electron microscope (SEM) and electron probe microanalyzer (EPMA). Preserved subsurface samples representing oxidized unsaturated zone, the top of the dry-season saturated zone, and deeper sediment were freeze-dried prior to impregnation. Surficial river sediments and mica separates from deeper, air-dried sediments were also mounted. Sample orientation and bedding features were not preserved during mounting.

A JEOL-5800LV SEM equipped with an Oxford ISIS energy dispersive x-ray spectrometer (EDS) was operated at 20 keV and 0.1-1 nA current with a 10 mm sample working distance during analysis of these samples. The operational detection limit for arsenic in pyrite under these analytical conditions was approximately 8000 ppm. Secondary and backscattered electron imaging were used to observe textural and chemical variations within pyrite grains. Oxford ISIS digital imaging software was used to measure dimensions of the pyrite grains.

Following textural observations with the SEM, 156 sulfide mineral grains in eight samples were analyzed with a fully automated, five-wavelength spectrometer JEOL 8900 EPMA. Operating conditions were 10 keV accelerating voltage, 30 nA beam current (cup), and focused beam. A 10 keV accelerating voltage was selected to reduce the analysis volume to approximately 1?m, based on Monte Carlo

simulations. Fe, S, As, Cu, and Zn concentrations were quantified using peak counting times of 10 seconds for Fe and S and 60 seconds for As, Cu, and Zn. Upper and lower background counting times were half the peak count times for the respective elements. L?x-ray lines were analyzed for As, Cu, and Zn. Si and Mg were measured concurrently with EDS. Although the calculated As detection limit is approximately 100 ppm using the above conditions, values below 300 ppm were not reproducible, so an effective detection limit of 300 ppm was assigned. Precision of As measurements are within 3% relative. All data points containing Mg and Si, most likely intergrown clays, were removed from the data set because of the known interference of As L?radiation with Mg K?radiation.

3. RESULTS

3.1. Bulk Sediment Characteristics

Sediment recovered from the boreholes and surface at Rajoir and Srirampur are typically gray in color with a few notable exceptions. Active river sediment and shallow sediment collected during the dry season (January-April) are yellow-brown through the unsaturated zone (2-4 meters depth) (Breit et al., 2004). Intervals of deeper, yellow-brown sediment were recovered from both the Srirampur (46 m) and Rajoir boreholes (305 m). These brown sediments are attributed to erosional unconformities such as that recognized at the end of the Pleistocene (Umitsu, 1993).

Regardless of color, all sediment recovered is micaceous feldspathic arenite. Quartz is the most abundant mineral with minor amounts of plagioclase, potassium feldspar, biotite, chlorite and muscovite (Breit et al., 2006; 2007). The abundances of micas and chlorite increase with decreasing grain size. Constituents of the < 2 ?m fraction include mica/illite, chlorite, smectite, and kaolinite. Authigenic phases recognized during SEM examination of grain mounts include goethite in the brown sediment and pyrite, siderite and iron phosphate (vivianite?) in gray samples. The sediment is mainly medium to fine sand but ranges from clay to pebbly coarse sand. Borehole sediment collected at Rajoir is generally coarser than that recovered at Srirampur (Fig. 2).

Total arsenic, organic carbon, sulfur, and the amount of iron dissolved by the 0.5 N HCl extractions (Fe_{HCl}) are significantly greater in the Srirampur sediment than that recovered at Rajoir (Table 1). Total arsenic does not vary systematically with depth in either borehole (Fig. 2). Arsenic content is generally more abundant in sediments that contain larger amounts of sulfur, organic carbon and silt and clay (<62 ?m). A strong correlation of arsenic with abundance of silt and clay is evident in the Rajoir borehole but is not apparent in the Srirampur sediment samples. Similar organic carbon-arsenic associations are indicated elsewhere in Bangladesh (JICA, 2002; Meharg et al., 2006). Nonetheless, the best interelement correlation for arsenic is with sulfur ($r^2 = 0.56$; $p < 0.001$; excluding outliers with > 50 ppm arsenic that greatly increased r^2). The association of arsenic and sulfur varies vertically within the boreholes as evident by variations in the ratio of arsenic and sulfur (Fig. 3).

The abundance of sulfur in the surficial and shallowest samples is directly related to the degree of water saturation. Sediment collected from surface excavations showed that saturated, gray sediment contains greater sulfur concentrations (median = 0.012 wt.%, n=6) than overlying unsaturated, brown sediment (median <0.005 wt.%, n = 8) and active river sediment (<0.005 wt.%). Sediment collected 0.5 meters below the shallow gray-brown interface at Rajoir contains 0.14 wt. % sulfur while sediment at a similar depth in Srirampur contains 0.01 wt. % sulfur. Arsenic in the shallow sediment is consistently <10 ppm and does not significantly correlate with sulfur.

Gray sediment from both study areas contains high contents of iron soluble in 0.5 N HCl (Table 1), which consistently has a Fe^{2+}/Fe_{total} ratio greater than 0.85 (Fig. 2; Breit et al., 2006; 2007) similar to previous results reported on sediments from elsewhere in Bangladesh (Horneman et al., 2004; van Geen et al., 2006). Much of the extracted iron is attributed to fine-grained siderite that was detected by XRD and SEM (Breit et al. 2006; 2007). The abundance of ferrous iron in the gray sediment contrasts with the content in the sediment within a few meters of the ground surface which typically has Fe^{2+}/Fe^{total} ratios < 0.2 (Breit et al., 2004). Buried brown sediment typically has a ratio < 0.5 (Horneman et al., 2004) but in this study was found to be <0.8 (Breit et al., 2006). The amount of total iron extracted by 0.5 N HCl

(Fe^{2+}_{HCl}) was used to approximate the degree of sulfidization assuming that all of the measured bulk sulfur was contained in pyrite. The ratio of $Fe_{pyrite}/Fe^{2+}_{HCl}$ ranged from 0.004 to 0.5 with a median of 0.1, which indicates that all samples contain iron in excess needed to form pyrite. The amount of iron extractable by Ti^{3+}-EDTA from the Srirampur sediment was consistently < 20% of the iron extracted by 0.5 N HCl (Breit et al., 2006).

The amount of arsenic chemically extracted from the Srirampur sediment is summarized in Figure 4. The lack of specificity of chemical extractions limits interpretation but the contrast in measured arsenic abundances among the extracts is consistent with other analyses used in this study. The arsenic in the 0.5 N HCl extracts may reflect absorbed arsenic and that bound in siderite and vivianite as suggested by the XAFS data (discussed in section 3.3). The release of arsenic by a reductive extraction (Ti^{3+}-EDTA) supports the presence of residual ferric oxides in the sediment. Samples from depths < 120 m tend to contain arsenic extractable by Ti^{3+}-EDTA that is either greater than or equal to the amount extracted by 0.5 N HCl , which contrasts with the results from the deeper samples. The median content of arsenic dissolved by Ti^{3+}-EDTA was 22% of the total extracted arsenic in sediment < 120 m while the median value in deeper sediment was 9%. In nearly all gray sediments, the oxidative extraction of H_2O_2-HCl dissolved more arsenic than the other extractions, which is consistent with the greatest content of arsenic in sulfide phases (Fig. 4).

3.2. Sulfur speciation and sulfur isotope composition

The abundances of AVS, pyritic sulfur (PY), and acid-soluble sulfate and their isotopic compositions are summarized in Figure 5 and listed in Table EA-1. Pyritic sulfur abundances vary from 20 to 9580 ppm (Fig. 5a) with the greatest concentrations detected in samples > 100 m deep at Srirampur. In contrast, the highest pyrite content at Rajoir was measured in the top two samples. Contents of PY are greater than AVS in 23 of 25 samples. The ratio of AVS to PY in samples from Srirampur decreases downward from shallow depths to 150 m. Below 150 m the ratios are <0.1 with the exception of 2 samples (Fig. 5b). These samples are notable for their low content of pyritic sulfur, and therefore the

calculated ratios are sensitive to small differences in concentration and analytical error. Sediment from Rajoir has generally greater AVS/PY values than Srirampur samples. Measurable sulfate was recovered from 16 of the 25 samples but at concentrations lower than associated sulfide (<10 to 130 ppm).

?^{34}S values vary widely with similar ranges for all forms; AVS varies from -13.8 to 39.9 per mil, the range for pyrite is -22.7 to 32.9 per mil (Fig. 5c), and the acid-soluble sulfate recovered varies from -13.5 to 35.3 per mil. Pyrite in 14 samples contains sulfur with an isotopic composition between +6 and -6 per mil including the samples at the top of the saturated zone (-0.4 and -2.3). Exceptions to this tendency are the two deepest samples from Srirampur and the shallowest borehole sample from Rajoir, which have ?$^{34}S_{PY}$ < -9 per mil. These samples also contain the greatest amount of pyritic sulfur of the samples analyzed. Eight samples have ?$^{34}S_{PY}$ > +8 per mil and 6 of these are in the upper 150 m of the boreholes. The isotopic composition of AVS (?$^{34}S_{AVS}$) was compared to pyrite (?$^{34}S_{PY}$) by calculating the difference for each sample (Fig. 5d). The absolute value of the difference for most samples is less than 6 per mil. In four samples from <50 m depth, ?$^{34}S_{AVS}$ is much greater than ?^{34}S values of pyrite. Two samples between 200 and 300 m depth have ?$^{34}S_{AVS}$ much less than ?$^{34}S_{PY}$. ?$^{34}S_{SO4}$ is greater than 14 per mil for all but one sample at 327 m depth at Srirampur (-13.5 per mil), which is very similar to the coexisting AVS. Four of the sulfate samples are in the depth range in which contamination from barite in the drilling mud is possible (>230 m) (Breit et al., 2006; 2007). However, the affect of contamination is considered minor because the measured ?^{34}S values are substantially different from the mud additive (Table EA-1).

3.3. Arsenic valence and solid phase speciation

The nominal arsenic valence values of Rajoir and Srirampur bulk sediment range from -0.2 to 2.2 (average: 1.1, n = 6) (Fig. 6), which indicates that reduced arsenic is the dominant form in these samples. Arsenate and arsenite typically constitute < 50 % of the total arsenic in bulk XANES and extended microXANES fits (Table 2). Partial oxidation of the samples during handling, transport and storage of

the samples may account for some or all of the arsenate, but our analyses of the oxidation state of 0.5 N HCl soluble iron and the abundance of AVS suggest oxidation was minimal. If the calculated abundance of arsenate in the deeper sediments is correct, then it is likely that some grains contain refractory oxidized arsenic that survived burial in the generally reducing environment of the gray sediment.

Progressive change of arsenic valence in the shallow (< 150 m depth) Srirampur aquifer sediment is evident in fits of bulk XANES spectra. These spectra integrate over the arsenic residence in hundreds to thousands of grains, including arsenic-rich pyrite that is typically 10 – 20 ?m in diameter and the more abundant, lower-arsenic grains of siderite, vivianite, HFO, and potentially other unrecognized phases that are typically associated with altered iron micas. Analysis of bulk XANES spectra indicates that the amount of sulfide arsenic is at a minimum at 22 m depth, increases by about 40% at 83 m, and again by 24% at 260 m depths, before leveling off to 71%, whereas arsenate is at a maximum in the shallowest sample, and is significantly (> 10%) less in the deeper samples. The trend for arsenite is less clear but there is a significant increase between 22 and 83 m depth with generally lowers values at greater depth. Overall, these spectra indicate that several phases and oxidation states of arsenic coexist in sediments, but that the relative proportions of these phases and oxidation states change with depth, in concert with overall changes in sediment geochemistry.

The models which minimized $?^2$ based on a linear combination least-squares fit to bulk XANES and extended microXANES spectra were arsenian pyrite, orpiment, siderite, vivianite, HFO, and HAO (Table 2 and EA Appendix-1). The use of arsenian pyrite, siderite, vivianite, and HFO in evaluating the data is consistent with SEM and extraction results (Fig. 4). HAO is justified as a fit component based on the weathering of abundant mica present in the samples. Arsenian pyrite was the most common component detected in sediment with low valent arsenic (Table 2). Orpiment was only detected in a bulk XANES spectrum of a shallow peat layer sampled in an excavation near Rajoir, a bulk XANES spectrum of Srirampur sediment from 29.1 m depth, and a microXANES spectrum of a grain in Srirampur sediment from 39 m depth. These findings do not preclude the possibility that both pyrite and orpiment are present

in some samples at concentrations below detection (about 5-10% of the total arsenic). For both the arsenian pyrite and orpiment species determinations, greater confidence is placed in the fits to extended microXANES spectra than fits to the bulk XANES spectra because the latter spectra contain less noise and have more data than the former. The low abundance of arsenite and arsenate solid-phase species and noted similarities among the XANES spectra of many arsenate/arsenite model compounds (Foster, 2003), makes these species assignments less certain.

Extended microXANES spectra from the Srirampur borehole are not representative of the overall arsenic speciation, but they provide the most detailed and reliable information on the identity of the solid-phase species of arsenic. Nearly all of the high As areas displayed on a false-color microXRF map have extended XANES spectra consistent with arsenian pyrite, with a small amount of oxidized arsenate in some spectra (Fig. 7, Table 2). No variation in the arsenian pyrite species could be observed between grains high in sulfur and low in arsenic or vice versa (Fig. 7a and b), but spots low in arsenic and sulfur (such as spot 5 in Fig. 7a, probably a mica grain based on the high K content) contain more arsenate and/or arsenite relative to arsenian pyrite, although the latter is still detected (see spot 5 XANES spectrum in Fig. 7d). Since the "micro" x-ray beam employed was rather large (16 x 7 ?m) relative to the size of the authigenic siderite and vivianite (as estimated from SEM images), it is likely that the spectrum collected at this spot is an integration over several, but not hundreds of discrete grains. Even with the knowledge that the sampling at spot 5 may not be representative of the arsenic speciation as a whole, the agreement is striking between the microXANES spectrum of spot 5 and the bulk sediment XANES spectrum from the same depth horizon, and suggests that this modal proportion of arsenic species is probably the most representative of the sample as a whole.

The arsenite and arsenate-bearing model compounds providing the best fits to the oxidized arsenic in extended microXANES spectra were siderite and vivianite; only two of the 12 spots examined at the 39 and 326 m depth intervals employed HFO in a fit (as an arsenite-HFO coprecipitate; see EA Appendix 1). This is in marked contrast to the bulk XANES fits, where HAO and HFO model compounds

provided the best fit in the majority of analyses (the only exceptions are the 326 and 355 depth intervals, in which arsenite coprecipitated with siderite is the preferred arsenite model). However, due to the high noise content of the bulk XANES spectra, it is impossible to assess whether the use of a different species in the least squares fits to these spectra is significant. There was no consistency to or trend in the particular arsenite and arsenate model compounds providing the best fits to the extended microXANES spectra. The intrinsic limitations of the information provided in the arsenite and arsenate XANES spectra is certainly a factor, but the non-representative nature of this type of analysis might also give rise to differences between fits to bulk and micro-XANES spectra.

3.4. Sulfide textures and morphology

Polished grain mounts examined with the SEM contain authigenic and sparse detrital sulfide mineral grains. The distinction between authigenic and detrital origin was based on grain morphology. Grains with broken and/or rounded edges were classified as detrital; although some abrasion may have occurred during drilling and handling of the samples. Framboids and euhedral forms were classified as authigenic. Although transport of framboidal forms has been observed (Hossain, 1975; Damke et al., 1999), their transport in Bangladesh likely represents local reworking rather than distant transport because pyrite will not survive weathering processes in the wet and oxidizing environment of the Bengal region (Nickson and et al. 2000).

Pyrite, and trace amounts of Zn-Cu-rich pyrite, pyrrhotite, sphalerite, and chalcopyrite were detected during the SEM examination. Arsenopyrite and other arsenic-containing minerals, such as orpiment and realgar, proposed by Das et al. (1996) and Chowdhury et al. (1999) were not detected, but XAFS spectroscopy suggests that orpiment may be present. No authigenic pyrite was detected in the river sediment, although rare detrital grains, 10-20 ?m in diameter are present. Authigenic pyrite, both framboidal and massive, is abundant in gray samples, especially in those collected from depths greater

than 50 m. Pyrite intergrowths with biotite and chlorite were common in the gray sediment, but were not observed in the river sands, in shallow unsaturated sediments, or within Fe deficient micas.

More than 90% of pyrite grains analyzed by EPMA are classified as authigenic using the guidelines described above. Atomic ratios of iron and sulfur calculated from electron probe analyses (Table EA-2) and x-ray diffraction confirm the iron sulfide phase to be pyrite as opposed to marcasite, mackinawite, or greigite. Although Akai et al. (2004) report greigite at ~49 m in western Bangladesh, it was not detected in this study. Authigenic FeS was observed only in a shallow sample collected at Srirampur where it formed a ~7 ?m massive rim on framboidal pyrite.

Framboid diameters range from 2 to 50 ?m with an average diameter of ~10 ?m. Crystallites, either spherical or octahedral, comprising individual framboids are of uniform size and shape and average 1 ?m in diameter. Framboidal pyrite was subdivided into open and filled categories dependent on how readily individual crystallites were distinguished. Open framboids are composed of isolated (non-touching) crystallites whose size and shape could easily be determined (Fig. 8a). Filled framboids contain intergown crystallites or voids between crystallites have been infilled with massive pyrite. Most framboids, regardless of being open or filled, are spherical. The few irregularly shaped framboids were distorted by compaction or by the space available for growth. Some framboids have been overgrown with massive or octahedral pyrite, particularly those in close vicinity to organic matter (Figs. 8b and 8c). Massive pyrite is divided into octahedral, cubic, and irregular forms. Octahedral (and cubic) crystals were found as overgrowths on framboids and as clusters of octahedra located near organic matter (Fig. 8d). The size of the octahedra ranges from 2 ?m to over 50 ?m. The irregular forms have features that suggest they grew in place because the delicate surface structures would not survive transport. The irregular forms range from 10 ?m to over 100 ?m. The most notable occurrence of an irregular form was found as massive pyrite replacing chloritized biotite in SH2-37 (Fig. 8e). Progressive replacement of biotite by authigenic pyrite was noted in several gray samples. Small framboids apparently nucleate well

within mica plates (Fig. 8f), progressively grow resulting in 'kinking' of the plates, and eventually become a massive replacement of the entire grain (Fig. 8e).

Massive and framboidal pyrite in the shallow sediment are similar to those in the deep sediment, with the exception that no massive forms were found in the shallowest samples in either borehole or the samples from the surface excavations (SP-5-1 and SP41-1). While morphologies were not restricted to specific depths, a few textural variations with depth were noted. The number of filled framboids increases with depth relative to open framboids. The size of the massive grains increases with depth although the number of samples is limited. Neither framboid and crystallite size of nor the relative number of framboidal and massive grains varied systematically with depth.

3.5. Arsenic content of pyrite

Arsenic content of pyrite grains as determined by electron microprobe is summarized in Tables 3 and EA-2. The inverse correlation of arsenic and sulfur is consistent with arsenic substitution for sulfur (Fig. 9). Observed scatter in arsenic atom percent at values less than 0.05 is attributed to higher error at low concentrations. A linear least squares fit for arsenic and sulfur for the massive varieties at Srirampur has an r^2 value of 0.675. In contrast, arsenic does not systematically substitute for sulfur in framboids based on the arsenic-sulfur r^2 value of 0.035. Similar As-S relations were detected in the Rajoir borehole.

The median arsenic content of the framboids is 1500 ppm with an observed range from <300 to over 11,000 ppm. Higher arsenic contents in framboids are associated with those found near organic matter and in mica- and clay-rich samples. Framboids within a sample have a range of arsenic contents, however multiple spot analyses within a framboid yielded similar arsenic contents. There is no systematic change in the arsenic content of framboids with depth, nor is there systematic difference in arsenic content in closed relative to open framboids (Table 3).

The median arsenic content of the massive pyrite is 3200 ppm with an observed range from <300 to 13,000 ppm arsenic. Massive overgrowths on arsenic-poor framboids generally contain between 2000 and 8000 ppm arsenic; some overgrowths contain as much as 10,000 ppm arsenic. The massive varieties

have higher arsenic contents than framboids (Fig. 10). Oscillatory arsenic zoning, with a range from <300 to over 13,000 ppm As, was observed in some of the octahedra, particularly those associated with organic matter (Fig. 8d). No systematic differences in the arsenic contents of octahedral, cubic, and irregular morphologies were observed.

The arsenic contents of pyrite from the Bengal basin sediments overlap with arsenic in pyrite preserved in other sedimentary units. Arsenic contents in natural pyrites range from 20-300 ppm in marine sediment, up to ~100 ppm in brackish settings, < 50 ppm in lacustrine settings, and as much as 10,000 ppm in coal (Schoonen, Table 2, 2004). Pyrites analyzed from the Black Warrior coal basin in Alabama contain from 3000 ppm to 4.5 weight percent arsenic (Goldhaber et al., 2003) and Kolker et al. (2003) report values up to 7 weight percent arsenic in authigenic pyrite in sandy glacial aquifers in southeastern Michigan. Although some of these occurrences are the product of diagenesis and fluid migration (T >25 °C), the importance of incorporating arsenic into pyrite is evident.

4. DISCUSSION

4.1. Arsenic in the Bengal Basin sediment

Arsenic speciation within the Bengal Basin sediment varies with depth. Breit et al. (2004) recognized that arsenic in shallow sediment above the water table is present as arsenate bound to iron oxides while the immediately subjacent gray, water-saturated sediment contains mainly As(III) bound to several phases and arsenic in pyrite. With increasing depth, arsenite and arsenate variably contained in siderite, vivianite, and sorbed to HFO and HAO-type phases persist with decreasing abundance (Table 2, Fig. 4). Ferric oxyhydroxides are of minor importance as an arsenic residence below ~100 m. Pyrite accounts for more than 70% of the arsenic in deep sediment (Table 2, Figs. 3 and 4). Polizzotto et al. (2005) similarly recognized that 60% of the total arsenic in the Holocene aquifer sediments (5 to 60 m) in central Bangladesh is incorporated in (unidentified) arsenic-bearing sulfides with the remaining portion in

arsenate- and arsenite-containing phases. Although empirically recognized as important, details of arsenic incorporation into pyrite has been only generally described.

4.2. Assimilation of Arsenic into Pyrite

Understanding the incorporation of arsenic into pyrite is inseparable from the arsenic form in the Bengal Basin pyrite and the fundamental processes of crystal growth. Previous XAS studies suggest that when arsenite is adsorbed to pyrite, an "arsenopyrite-like" surface precipitate is formed (Bostick and Fendorf, 2003), whereas when arsenic is incorporated into growing pyrite (under hydrothermal conditions, at least) it substitutes for sulfur in crystallographic sites (Savage et al., 2000). Since arsenopyrite and arsenian pyrite can be readily distinguished (see Appendix AE-1), our findings indicate that the majority of pyrite-associated arsenic was incorporated into pyrite concurrent with its formation. Inferred substitution of arsenic and sulfur is also evident in the microprobe data (Fig. 9). However, since dissolved arsenite is present in ground water in contact with these pyrite-rich sediments, it is possible that the arsenian pyrite is coated with arsenopyrite-like surface precipitates. The quality of the microXANES spectral fits using arsenian pyrite alone (fit totals near 100% for most samples) suggest that an arsenopyrite-like surface precipitate, if present, is of minor abundance.

The presence of arsenian pyrite and possibly orpiment are consistent with calculated thermodynamic stabilities. Arsenic phases predicted to be stable in contact with water compositions typical of those recovered from gray Holocene sediment (BGS-DPHE, 2001) were evaluated with Geochemist's Workbench. The thermo.com.v8.v6.full database was modified with arsenic thermodynamic data of Nordstrom and Archer (2003) and Pokrovski et al. (2002); thioarsenite species were suppressed based on the abundance of reactive iron in the sediment (Wilkin et al., 2003). The stability of arsenian pyrite was approximated by the stabilities of arsenopyrite and pyrite because thermodynamic data for arsenian pyrite is not available. Also, pyrite is kinetically favored to form relative to direct precipitation of FeAsS (Fleet et al., 1989) as reflected in many of the octahedral pyrite grains that have As zoning (Fig. 8d). As expected, ground waters are saturated with arsenopyrite and

pyrite at the circumneutral pH of most Bangladesh ground water. Orpiment dominance is predicted in water with pH <6 and dissolved iron content less than 0.5 mg L^{-1}. These conditions are likely in carbonaceous sediments that have elevated pCO_2 and lack clastic iron input such as the peaty sediment near Rajoir.

The concentration of arsenic in pyrite is the product of growth rate, the abundance of arsenic in solution, and the dissolved As:S ratio (Bostick and Fendorf, 2003; Fleet et al. 1989). Akai et al. (2004), Kirk et al. (2004), and O'Day et al. (2004) have proposed that arsenic incorporation into iron sulfide is dependent on the rate of sulfur supplied by bacterial sulfate reduction. Arsenic incorporation in pyrite is expected to increase in response to lowered sulfur activities found in Bengal Basin sediment deeper than 20 meters (Fig. 11). As sulfur is depleted, pore waters cease to be supersaturated and pyrite growth becomes more prevalent than nucleation, which results in euhedral morphologies (Wang and Morse, 1996; Grimes et al., 2002; Sawlowicz, 2000). Under conditions of slower growth, greater content of arsenic in the pyrite is likely based on results of Bostick and Fendorf (2003) who found that arsenic sorption to pyrite increased with longer exposure to arsenic-rich solutions. The massive pyrite common in deeper samples generally contains more arsenic than associated framboids (Fig. 10), an observation that is not unique to the pyrite in Bengal Basin sediment (Goldhaber et al., 2003; Kolker et al., 2003).

Framboidal pyrite is favored in the upper 20 m of Bengal Basin borehole sediment because of rapid precipitation rates in settings with adequate supplies of both Fe and S (Wang and Morse, 1996; Grimes et al., 2002). Consistent with this interpretation framboids were the only morphology observed in the gray sediment from excavations and the borehole samples from <22 m. The uniform content of arsenic within an individual framboid suggests the crystallites formed under similar pore-water compositions that sustained nucleation and growth (Matijevic, 1996; Wilkin and Barnes, 1997). The variation in arsenic content among framboids within a sample is attributed to heterogeneity of the sediment or microniches of varying saturation states (Diehl et al., 2005; Grimes et al., 2002; Sawlowicz, 2000).

Although useful, these findings do not shed light on the many unanswered questions regarding the mechanism and timing of low temperature pyrite formation (e.g., Butler and Rickard, 2000). However, some information is gleaned from the bulk chemical data and textural observations of Bengal Basin pyrite. The pyrite most likely forms via at least two mechanisms. The first is conversion of AVS to pyrite as indicated by the AVS to pyrite ratio which decreases with depth (Fig. 5). Although the sediment is undersaturated with respect to AVS but saturated with respect to pyrite, extraction results indicate more iron is available than needed to form pyrite which will enable formation of AVS (Schoonen, 2004). The second possible method of pyrite formation is through heterogeneous nucleation on surfaces without amorphous FeS precursors. This is evident from the formation of pyrite framboids within the sheets of iron-rich micas which eventually grow to replace the entire mica grain (Fig. 8e). Rickard et al. (2007) were able to nucleate pyrite framboids within the cell walls of celery via a two step process whereby Fe(II) diffusion and subsequent S(-II) penetrate and react within the cell walls. Once formed, the pyrite seeds act as nucleation sites to facilitate further pyrite growth (Schoonen, 2004; Rickard et al., 2007).

4.3. Sulfur supply

Multiple sources of sulfur are necessary to reasonably explain the isotopic composition and abundance of sulfur forms in the sediment. Natural sources of sulfate available for reduction within the Bengal Basin sediment include oxidation of detrital sulfides, atmospheric deposition, river water, and sea water. Detailed evaluation of these sources is described in the EA Appendix 2 and summarized in Figure 12. The median amount of sulfur in the sediment (Table 1) exceeds the amount that can be supplied by atmospheric deposition or redistribution of sulfur in existing surficial sediment based on likely rates of sediment accumulation (0.1 to 1 cm a^{-1}). Therefore, riverine and seawater inputs are required. To refine this conclusion, three groups of sediment samples were evaluated using the results of the sulfur isotope and sulfur speciation analyses (Fig. 5). The first group has $?^{34}S$ values between +6 and -6 per mil and

pyritic sulfur (S_{PY}) concentration between 60 and 1000 ppm. These values are consistent with a riverine sulfur supply that would increase the sediment sulfur content to between 100 and 1300 ppm S depending on the rate of sediment deposition. The second population consists of 7 samples with $?^{34}S_{PY}$ values from 8 to 32 per mil and S_{PY} contents ranging from 40 to 1100 ppm. Although these results can be explained by advective transport of partially reduced riverine sulfate to a site of further reduction, a limited supply of seawater sulfate offers a simpler explanation. A seawater source is particularly favored to explain a sample from Srirampur at 114.5 m depth that contains 1090 ppm S_{PY} with a $?^{34}S_{PY}$ of 29.2 per mil. The third population includes 3 samples with > 1500 ppm S_{PY} and $?^{34}S$ values < -9 per mil, which is explained by a sulfate source of high concentration that was only partially reduced. The high abundance of sulfur and low $?^{34}S_{PY}$ values render sea water the most likely source of sulfate and that the amount of sulfate exceeded the reducing capacity of the sediment.

The two shallowest samples from the Rajoir borehole are examples of populations 2 and 3. Sediment at 11 m depth contains the greatest amount of measured S_{PY} (1 wt.%). This pyrite has a $?^{34}S$ value of -9.1 per mil and is associated with +35 per mil sulfate. In contrast, a sample at 22 m depth contains S_{PY} of 350 ppm and a $?^{34}S_{PY}$ of +33 per mil. The simplest explanation for this distribution is that sea water interacted directly with the carbonaceous sediment at 11 m and that residual, isotopically evolved sulfate was transported in ground water downward through the sediment and was further reduced to form pyrite in the sediment at 22 m. Exposure of sediment in this depth range to sea water is consistent with the estimated coastline position near Rajoir 6 to 3 ka BP (Goodbred and Kuehl, 2000).

The difference between $?^{34}S_{AVS}$ and $?^{34}S_{PY}$ in most sediment samples is positive or close to zero (Fig. 5d). Positive values are attributed to initial formation of ^{34}S depleted pyrite and subsequent formation of AVS from the ^{34}S enriched reservoir. Samples in the upper 50 m of both boreholes have this characteristic. In contrast, samples in the vicinity of 200 to 300 m depth at Srirampur have lower $?^{34}S_{AVS}$ values which imply addition of sulfate in ground water subsequent to formation of most pyrite in those samples. Perhaps sea water intrusion affected this interval after much of the pyrite had formed.

The sulfur isotope composition of dissolved sulfate ($?^{34}S_{SO4-D}$) in Bangladesh ground water further supports multiple sulfate sources. $?^{34}S_{SO4-D}$ determined by BGS and DPHE (2001) and Zheng et al. (2004) ranges from -0.9 to 53 per mil. $?^{34}S_{SO4-D}$ values < 5 per mil are attributed to oxidation of authigenic sulfide as is likely to explain the acid-soluble sulfate deep (326.5 m) in the Srirampur borehole (-13.4 per mil). Although the data of BGS and DPHE (2001) and Zheng et al. (2004) show that $?^{34}S_{SO4-D}$ generally increases with decreasing concentration as expected for bacterial sulfate reduction (Lyons, 1997; Schoonen, 2004, Zheng et al., 2004), the large range of 0 to 26 per mil measured in a narrow sulfate concentration range (10 to 20 mg L^{-1}) is greater than expected for any single source outlined above.

The markedly low As/S ratios in the sediment (Fig. 3) between approximately 20 and 50 meters at Srirampur and to a lesser degree at Rajoir are considered a direct reflection of depositional conditions. The brown sediment at 50 m depth marks the position of the Holocene-Pleistocene unconformity in the Srirampur borehole. Goodbred and Kuehl (2000) and Acharyya (2005) proposed that following the unconformity, sea level rose as fast as 1 – 2 cm yr^{-1} from 12 to 6 ka BP resulting in rapid aggradation of sediment. Rapid sediment deposition between 50 and 20 m depth effectively diluted the sulfur fluxes, particularly because sea water input was unlikely. Applying the riverine and atmospheric fluxes to sediment accumulating at 1 cm yr^{-1} would result in sediment with concentrations of sulfur less than 0.01 wt.% S while arsenic provided in ferric oxyhydroxide grain coatings likely remained constant. From 6 to about 3 ka BP the aggradation of sediment reduced sharply and further declined after 3000 years BP (Goodbred and Kuehl, 2000). Deposition at slower rates near 0.1 cm yr^{-1} is likely to produce sulfur concentrations near 0.1 wt.% with riverine input, which is similar to the value measured in some of the slowly deposited sediment in the upper 20 m. The shallowest Rajoir sediment is marked by very low As/S ratios which is attributed to a large influx of sulfur from sea water. The relative lack of sulfur in sediment between 50 and approximately 100 m could be related to circulation of dilute ground water in response to the position of sea level 120 m below the current mean sea level at the end of the Pleistocene (Ravenscroft and McArthur, 2004). Alternatively, the lower sulfur content could reflect depositional

conditions during the Pleistocene, which limited sulfur content much as it was limited in the lower Holocene. Full interpretation of the sediment at > 50 m depth requires a more complete description of depositional environments and rates of accumulation.

5. SUMMARY

Pyrite has a major role in the arsenic geochemistry in the sediment of the Bengal Basin. Arsenian pyrite weathering in rocks and sediment from the Himalayas adds to the arsenic load of modern sediments in the form of ferric oxides that coat grain surfaces. Reducing conditions in the subsurface dissolve ferric oxides and release contained arsenic. In the presence of adequate sulfate, the dissolved arsenic is partitioned into pyrite. Framboids form near the top of the saturated zone while massive textures form deeper in the sediment in response to slower growth attributed to limited sulfate. Higher dissolved arsenic:sulfur ratios are likely in the deeper sediment which favors incorporation of proportionally greater amounts of arsenic into the massive pyrite. Pyrite abundance in deep sediment and active sulfate reduction in very shallow sediment could account for the generally low concentration of arsenic in ground water from those depth intervals.

Acknowledgements- This research was carried out under contract with the United States State Department and funding support from USAID. The authors thank Cyrus Berry, Dave Siems, Tammy Hannah, Zoe Ann Brown, Rhonda Driscoll, Paul Briggs and David Fey for the chemical analyses. Michele Tuttle, Sharon Diehl, Robert Zielinski, Alex Van Geen and two anonymous reviewers who offered insightful comments that greatly improved the clarity of the manuscript. The dedicated drilling crews of the Geological Survey of Bangladesh and Bangladesh Water Development Board made borehole sampling possible. The Stanford Synchrotron Radiation Laboratory is a national user facility operated by Stanford University on behalf of the U.S. Department of Energy, Office of Basic Energy Sciences. The SSRL Structural Molecular Biology Program is supported by the Department of Energy, Office of Biological and Environmental Research, and by the National Institutes of Health, National Center for Research

Resources, Biomedical Technology Program. The ALS is supported by the Director, Office of Energy Research, Office of Basic Energy Sciences, Materials Sciences Division of the U.S. Department of Energy, under Contract No. DE-AC02-05CH11231.

References

Acharyya S.K. (2002) Arsenic contamination in groundwater affecting major parts of southern West Bengal and parts of western Chhattisgarh: Source and mobilization process. *Current Science* **82,** 740-744.

Acharyya S.K. (2005) Arsenic levels in groundwater from Quaternary alluvium in the Ganga Plain and the Bengal Basin, Indian Subcontinent: Insights into Influence of stratigraphy. *Gondwana Research* **8** 55-66.

Acharyya S.K., Lahiri S, Raymahashay B.C. and Bhowmik A. (2000) Arsenic toxicity of groundwater in parts of the Bengal basin in India and Bangladesh: the role of Quaternary stratigraphy and Holocene sea-level fluctuation. *Environ. Geol.* **39**, 1127-1137.

Akai J., Izumi K., Fukuhara H., Masuda H., Nakano S., Yoshimura Ohfuji H., Anawar H.M. and Akai K. (2004) Mineralogical and geomicrobiological investigations on groundwater arsenic enrichment in Bangladesh. *Appl. Geochem.* **19**, 215-230.

Allison M.A. (1998) Geological framework and environmental status of the Ganges-Brahmaputra Delta. *J. Coastal Res*. **14** 825-836.

Berg M., Tran H.C., Nguyen T.C., Pham H.V., Schertenleib R. and Giger W. (2001) Arsenic contamination of groundwater and drinking water in Vietnam: A human health threat. *Envrion. Sci. Tech.* **35**, 2621-2626.

BGS and DPHE (2001). In Kinniburgh D.G. and Smedley P.L. (Eds) Arsenic Contamination of groundwater in Bangladesh. BGS Technical Report WC/00/19, British Geological Survey, Keyworth.

Bostick B.C. and Fendorf S. (2003) Arsenite sorption on troilite (FeS) and pyrite (FeS2). *Geochim. Cosmochim. Acta,* **67**, 909-921.

Breit G. N., Foster A.L., Perkins R.B., Yount J.C., King Trude, Welch A.H., Whitney J.W., Uddin N., Muneem A.A. and Alam M. (2004) As-rich Ferric oxyhydroxide enrichments in the shallow

subsurface of Bangladesh, In Wanty R.B. and Seal R.R. II., (Eds.) *Proceed. 11th Internat. Symp. Water-Rock Interaction* WRI-11, Balkema, New York, 1457-1461.

Breit G.N., Yount J.C., Uddin M.N., Muneem A.A., Lowers H.A., Driscoll R.L. and Whitney J.W. (2006) Compositional data for Bengal delta sediment collected from boreholes at Srirampur, Kachua, Bangladesh. U.S. Geol. Surv. Open-file Report 2006-1222, 58p.(http://pubs.er.usgs.gov/usgspubs/ofr/ofr20061222)

Breit G.N. Yount, J.C., Uddin M.N., Muneem A.A., Lowers H.A., Berry C.J., and Whitney J.W. (2007) Compositional data for Bengal delta sediment collected from a borehole at Rajoir, Bangladesh. U.S. Geol. Surv. Open-file Report 2007-1022, 46p. http://pubs.er.usgs.gov/usgspubs/ofr/ofr20071022

Butler I.B. and Rickard D. (2000). Framboidal pyrite formation via the oxidation of iron (II) monosulfide by hydrogen sulfide. *Geochim. Cosmochim. Acta* **64**, 2665-2672.

Chatterjee A.D., Das D., Mandal B.K., Chowdhury T.R., Samanta G. and Chakraborty D. (1995) Arsenic in groundwater in 6 districts of West Bengal, India—the biggest arsenic calamity in the world. A. Arsenic species in drinking water and urine of affected people. *Analyst* **120**, 643-650.

Chowdhury T.R., Basu G.K., Mandal B.K., Biswas B.K., Samanta G., Chowdhury UK, Chanda CR, Lodh D, Lal Roy S., Saha K.C., Roy S., Kabir S., Quamruzzaman Q. and Chakraborti D. (1999) Arsenic poisoning in the Ganges delta. Comment No. 2. *Nature* **401**, 545-546.

Clesceri L.S., Freenber A.E. and Eaton A.D., eds. (1998) 3500-Iron B. Phenanthroline method in Standard Methods for the Examination of Water and Wastewater 20th edition: Washington D.C., American Public Health Association, 3-76 - 3-78.

Damke H., Henning K.H., Lehmann J., Kasbohm J. and Puff T. (1999) Phase composition of flood sediments of the German-Polish Odra river immediately after the flood event in 1997. *Acta Hydrochim. Hydrobiol.* **27**, 357-363.

Das D., Samanta G., Manda, B.K., Chowdhury T.R., Chanda C.R., Chowdhury P.P., Basu G.K. and Chakraborti D. (1996) Arsenic in groundwater in six districts of West Bengal, India. *Environ. Geochem. Health* **18**, 5-15.

Diehl S.F., Goldhaber M.B., Tuttle M.L.W., Ruppert L.F., Hatch J.R., Koenig A.E. and Lowers, H.A. (2005) Concentration of arsenic, selenium, and other trace elements in pyrite-filled structures in Appalachian coals of Alabama, Kentucky, and West Virginia. Proceedings of the 22nd International Pittsburg Coal Conference; Coal Chemistry, Geosciences Resources, Sept. 12-15, Pittsburgh, PS, CD ROM, 24p.

Farmer J.G. and Lovell M.A. (1986) Natural enrichment of arsenic in Loch Lomond sediments: *Geochim. Cosmochim. Acta* **50**, 2059-2067.

Fleet M.E., MacLean P.J. and Barbier, J. (1989) Oscillatory-zoned As-bearing pyrite from stratabound and stratiform gold deposits: an indicator of ore fluid evolution. *Economic Geology Monograph* **6**, 356-362.

Foster A. L. Brown G. E., Jr. and Parks G. A. (1998a) X-ray absorption fine structure spectroscopy study of photocatalyzed, heterogeneous As(III) oxidation on kaolin and anatase. *Environ. Sci. Technol.* **32**, 1444-1452.

Foster A. L. Brown G. E., Jr., Parks G. A. and Tingle T. N. (1998b) Quantitative speciation of arsenic in mine tailings using X-ray absorption spectroscopy. *Amer. Mineral.* **89**, 553-568.

Foster A. L. (1999) Partitioning and transformation of arsenic and selenium in natural and laboratory systems. Ph.D. Thesis, Stanford University.

Foster A.L. (2003) Spectroscopic investigations of arsenic species in solid phases. In: Welch A.H. and Stollenwerk K.G. (Eds.), Arsenic in Groundwater: Geochemistry and Occurrence. Kluwer Academic Publishers, Norwell, 475 p.

Galy A. and France-Lenard C. (1999) Weathering processes in the Ganges Brahmaputra basin and riverine alkalinity budget. *Chem Geol.* **159**, 31-60.

Goldhaber M.B., Lee R.C., Hatch J.R., Pashin J.C. and Treworgy J. (2003) Role of large scale fluid-flow in subsurface arsenic enrichment. In: Welch A.H. and Stollenwerk, K.G. (Eds.), Arsenic in Groundwater. Kluwer Academic Publishers, 127-164.

Goodbred S.L., Jr. and Kuehl S.A. (2000) The significance of large sediment supply, active tectonism, and eustasy on margin sequence development: Late Quaternary stratigraphy and evolution of the Ganges—Brahmaputra delta. *Sed. Geol.* **133**, 227-248.

Grimes S.T., Davies K..L., Butler I.B., Brock F., Edwards D., Rickard D., Briggs D.E.G. and Parkes R.J., (2002) Fossil plants from the Eocene London Clay: the use of pyrite textures to determine the mechanism of pyritization. *J. Geol. Soc. London* **159**, 493-501.

Harvey C.F., Swartz C.H., Badruzaman A.B.M., Keon-Blute N., Yu W., Ali M.A., Jay J., Bechie R., Niedan V., Brabander D., Oates P.M., Ashfaque K.N., Islam S., Hemond H.F. and Ahmed M.F. (2002) Arsenic mobility and groundwater extraction in Bangladesh. *Science* **298**, 1602-1606.

Heron G. and Christensen T.H. (1995) Impact of sediment-bound iron on redox buffering in a landfill leachate polluted aquifer, (Vejen, Denmark). *Environ. Sci. Tech.* **29,** 187 -192.

Hideki Minami and Yoshihisa Kato (1997) Remobilization of arsenic in sub-oxic sediments from the seafloor of the continental margin. *J. Ocean*. **53**, 553-562.

Horneman A., Van Geen A., Kent D.V., Mathe P.E., Zheng Y., Dhar R.K., O'Connell S. Hoque M.A., Aziz Z., Shamsudduha M., Seddique A.A. and Ahmed K.M. (2004) Decoupling of As and Fe release to Bangla desh groundwater under reducing conditions. Part 1.: Evidence from sediment profiles. *Geochem. Cosmochim. Acta* **68**, 3459-3473.

Hossain A. (1975) The occurrence of polyframboidal pyrite in a beach sand deposit, Cox's Bazar, Bangladesh. *Amer. Mineral.* **60**, 157-158.

Huerta-Diaz M.A. and Morse J.W. (1992) Pyritization of trace metals in anoxic marine sediments: *Geochem. Cosmochim. Acta* **56**, 2681-2702.

Huerta-Diaz M.A., Tessier A. and Carignan R. (1998) Geochemistry of trace metals associated with reduced sulfur in freshwater sediments. *Appl. Geochem.* **13**, 213-233.

Islam, F.S, Gault, A.G., Boothman, C., Polya, D.A., Charnock, J.M., Chatterjee, D. and Lloyd, J. (2004) Role of metal-reducing bacteria in arsenic release from Bengal Delta sediments. *Nature (London)*, **430**, 68-71.

Islam, F.S., Boothman, C., Gault, A.G., Polya, D.A. and Lloyd, J.R. (2005) Potential role of the Fe(III)-reducing bacteria Geobacter and Geothrix in controlling arsenic solubility in Bengal delta sediments. *Min. Mag.* **69**, 865-875.

JICA-Japanese International Cooperation Agency (2002) The study on the ground water development of deep aquifers for safe drinking water supply to arsenic affected areas in western Bangladesh: Kokusai Kogyo Co., Ltd, and Mitsui Mineral Development Engineering Co., Ltd.

Kester C.L., Rye R.O., Johnson C.A., Schwartz Ch. and Homes Ch. (2001) On-line sulfur isotope analysis of organic material by direct combustion: preliminary results and potential applications. *Isotopes in Environmental Health Studies* **37**, 53-65.

Kirk M.F., Holm T.R., Park J., Jin Q., Sanford R.A., Fouke B.W. and Bethke C.M. (2004) Bacterial sulfate reduction limits natural arsenic contamination in groundwater. *Geology*, **32**, 953-956.

Kolker A., Haack S.K., Cannon W.F., Westjohn D.B., Kim M.J., Nriagu J. and Woodruff L.G. (2003) Arsenic in southeastern Michigan. In: Welch A.H., Stollenwerk, K.G. (Eds.), Arsenic in Groundwater. Kluwer Academic Publishers, 281-294.

Lyons T.W. (1997) Sulfur isotopic trends and pathways of iron sulfide formation in upper Holocene sediments of the anoxic Black Sea. *Geochim. Cosmochim. Acta* **61**, 3367-3382.

Marcus M. A., MacDowell A. A., Celestre R., Manceau A., Miller T., Padmore H. A. and Sublett R. E. (2004) Beamline 10.3.2 at ALS: a hard X-ray microprobe for environmental and materials sciences. *J. Synchrotron Radiation* **11**, 239-247.

Masuda H., Yamatani Y. and Okai M. (2005) Transformation of arsenic compounds in modern intertidal sediments of Iriomote Island, Japan. *J. Geochem Expl.* **87**, 73-81.

Matijevic E. (1996) Internally and externally composite monodispersed colloid particles. In: Pelizzetti, E. (Ed.), Fine Particles Science and Technology. Kluwer Academic Publishers, Boston, 1-12.

McArthur J.M., Banerjee D.M., Hudson-Edwards K.A., Mishhra R., Purohit R., Ravenscroft P., Cronin A., Howarth R.J., Chatterjee, A., Talukder T., Lowry D., Houghton S. and Chadha D.K. (2004) Natural organic matter in sedimentary basins and its relation to arsenic in anoxic ground water: the example of West Bengal and its worldwide implications. *Appl. Geochem.* **19**, 1255-1293.

Meharg, A.A., Scrimgeour, C., Hossain, S.A., Fuller, K., Cruickshank, K., Williams, P.N. and Kinniburgh, D.G. (2006) Codeposition of organic carbon and arsenic in Bengal delta aquifers. *Environ. Sci. Technol.* **40**, 4928-4935.

Moore J.N., Ficklin W.H. and Johns C. (1988) Partitioning of arsenic and metals in reducing sulfidic sediments. *Environ. Sci. Technol.* **22**, 432-437.

Mucci Alfonso, Richard L-F., Lucotte M. and Guignard Constance (2000) The differential geochemical behavior of arsenic and phosphorous in the water column and sediments of the Saguenay Fjord estuary, Canada. *Aquatic Geochem.* **6**, 293-324.

Nickson R.T., McArthur J.M., Ravenscroft P., Burgess W.G. and Ahmed K.M. (2000) Mechanism of arsenic release to groundwater, Bangladesh and West Bengal. *Appl. Geochem.* **15**, 403-413.

Nordstrom D.K. and Archer D.G. (2003) Arsenic thermodynamic data and environmental geochemistry. In: Welch A.H. and Stollenwerk K.G. (Eds.), Arsenic in Groundwater. Kluwer Academic Publishers, 1-26.

O'Day P.A., Vlassopoulos D., Root R. and Rivera N. (2004) The influence of sulfur and iron on dissolved arsenic concentrations in the shallow subsurface under changing redox conditions. *Proc. Nat. Acad. Sci.* **101**, 13703-13708.

Pirrie D., Beer A.J. and Camm G.S. (1999) Early diagenetic sulphide minerals in the Hayle Estuary, Cornwall, Williams, B.J., (Ed.). Geoscience in south-west England **9**, 325-332.

Pokrovski G.S., Kara Sami and Roux Jacques (2002) Stability and solubility of arsenopyrite, FeAsS, in crustal fluids. *Geochem. Cosmochim Acta* **66**, 2361-2378.

Polizzotto M.L., Harvey C.F., Sutton S.R. and Fendorf S. (2005) Processes conducive to the release and transport of arsenic into aquifers of Bangladesh. *Proceed. National Acad. of Sci.* **102**, 18819-18823.

Ravenscroft Peter (2003) Overview of the hydrogeology of Bangladesh, in Rahman A.A. and Ravenscroft P., Ground water resources and development in Bangladesh: Dhaka, Bangladesh, The University Press Limited.

Ravenscroft P. and McArthur J.M. (2004) Mechanism of regional enrichment of groundwater by boron: the examples of Bangladesh and Michigan, USA. *Appl. Geochem.* **19**, 1413-1430.

Ravenscroft P., Burgess W.G., Ahmed K.M., Burren Mellanie and Perrin Jerome (2005) Arsenic in groundwater of the Bengal Basin, Bangladesh: Distribution, field relations, and hydrogeological setting: *Hydro. Journal* **13**, 727-751.

Rice C.A., Tuttle M.L. and Reynolds R.L. (1993) The analysis of forms of sulfur in ancient sediments and sedimentary rocks: comments and cautions. *Chem. Geol.* **107**, 83-95.

Rickard D., Grimes, S., Butler, I., Oldroyd, A. and Davies, K.L. (2007) Botanical constraints on pyrite formation. *Chem. Geo.* **236**, 228-246.

Saunders J.A., Lee M.K., Uddin A., Mohammad S., Wilkin R.T., Fayek M. and Korte N.E. (2005a) Natural arsenic contamination of Holocene alluvial aquifers by linked tectonic, weathering, and microbial processes. *Geochem. Geophys. Geosystems* **6** (4).

Saunders, J.A., Mohammad, S., Korte, N.E., Lee, M.-K., Fayek, M., Castle, D. and Barnett, M.O. (2005b) Groundwater geochemistry, microbiology, and mineralogy of two arsenic-bearing Holocene alluvial aquifers from the USA. *Amer. Chem. Soc. Symp. Ser.* **915**, 191-205.

Saunders, J.A., Pritchett, M.A. and Cook, R.B. (1997) Geochemistry of biogenic pyrite and ferromanganese stream coatings: A bacterial connection? *Geomicrobiology J.* **14**, 203-217.

Savage K.S., Tingle T.N., O'Day P.A., Waychunas G.A. and Bird D.K. (2000) Arsenic speciation in pyrite and secondary weathering phases, Mother Lode Gold District, Tuolumne County, California. *Appl. Geochem.* **15**, 1219-1244.

Sawlowicz Z. (2000) Framboids: From their origin to application. Prace Mineralog. Pan (Krakow) (Mineralog. Trans.) **88**, 1-80.

Schoonen M.A.A. (2004) Mechanisms of sedimentary pyrite formation. In: Amend J.P., Edwards K.J., and Lyons T.W. (Eds.), Sulfur Biogeochemistry—Past and Present. *Geol. Soc. of America Spec. Pap.* **379,** 117-134.

Slowey A. J., Rytuba J. J. and Brown G. E., Jr. (2005) Speciation of mercury and mode of transport from Placer gold mine tailings. *Environ. Sci. Technol.* **39**, 1547-1554.

Southam, G. and Saunders, J.A. (2005) Geomicrobiology of ore deposits. *Econ. Geo.* **100**, 1067-1084.

Sternbeck John, Sohlenius Gustav and Hallberg R.O. (2000) Sedimentary trace elements as proxies to depositional changes induced by a Holocene fresh-brackish water transition. *Aquatic Geochem.* **6**, 325-345.

Stollenwerk K.G., Breit G.N., Welch, A.H., Yount J.C., Whitney J.W., Foster A.L., Uddin M.N., Majumder R.K., Ahmed Nasir (2007) Arsenic attenuation by oxidized sediments in Bangladesh. *Sci Total Env*. doi:10.1016/j.scitotenv.2006.11.029

Stuben Doris, Berner Zsolt, Chandrasekharam D. and Karmakar Julie (2003) Arsenic enrichment in groundwater of West Bengal India: geochemical evidence for mobilization of As under reducing conditions. *App. Geochem.* **18**, 1417-1434.

Sullivan K.A. and Aller R.C. (1996) Diagenetic cycling of arsenic in Amazon shelf sediments. *Geochim. Cosmochim. Acta* **60**, 1465-1477.

Swartz C.H., Blute N.K., Badruzzman B., Ali A., Jay J., Besancon J., Islam S., Hemond H.F. and Harvey C.F. (2004) Mobility of arsenic in a Bangladesh aquifer: inferences from geochemical profiles, leaching data, and mineralogical characterization. *Geochem. Cosmochim Acta* **68**, 4539-4557.

Taggart J.E. (2002) Analytical methods for chemical analysis of geologic and other materials, U.S. Geological Survey, *U.S. Geol. Sur. Open-file Report 02-223.* (Available at http://pubs.usgs.gov/of/2002/ofr-02-0223/OFR-02-0223.pdf

Tuttle M.L., Goldhaber M.B. and Williamson D.L. (1986) An analytical scheme for determining forms of sulfur in oil shales and associated rocks. *Talanta* **33**, 953-961.

Umitsu M. (1993) Late Quaternary sedimentary environments and landforms in the Ganges Delta. *Sed. Geol.* **83**, 177-186.

van Geen A., Rose J., Thoral S., Garnier J.M., Zheng Y. and Bottero Y.Y. (2004) Decoupling of As and Fe release to Bangladesh ground water under reducing conditions. Part II: Evidence from sediment incubations. *Geochim. Cosmochim. Acta* **68**, 3475-3486.

van Geen A., Zheng Y., Cheng Z., Aziz A., Horneman A., Dhar R.K., Mailloux B., Stute M., Weinman B., Goodbred S., Seddique A.A., Hoque M.A., Ahmed K.M. (2006) A transect of groundwater and sediment properties in Araihazar, Bangladesh: Further evidence of decoupling between As and Fe mobilization. *Chem, Geol.* **228** 85-96.

van Geen A., Zheng Y., Versteeg R., Stute M., Horneman A., Dhar R.K., Steckler M., Gelman A., Small C., Ahsan H., Graziano J., Hussein I. and Ahmed K.M. (2003) Spatial variability of arsenic in 6000 tube wells in a 25 km2 area of Bangladesh, *Water Res. Res.* **39** 1140 doi:10.1029/2002WR001617.

Walker S. R., Jamieson H. E., Lanzirotti A., Andrade C. F. and Hall G. E. M. (2005) The speciation of arsenic in iron oxides in mine wastes from the Giant gold mine, N.W.T.: application of synchrotron micro-XRD. *Can. Mineral.* **43**, 1205-1244.

Wang Q. and Morse J.W. (1996) Pyrite formation under conditions approximating those in anoxic sediments; I. Pathway and morphology. *Marine Chem.* **52**, 99-121.

Webb S. (2002) Sam's Interface for XAS Package (SixPACK) (available at http://www-ssrl.slac.stanford.edu/~swebb/sixpack.htm).

Wilkin R.T. and Barnes H.L. (1997) Formation processes of framboidal pyrite. *Geochim. Cosmochim. Acta* **61**, 323-339.

Wilkin R.T. and Ford R.G. (2002) Use of hydrochloric acid for determining solid-phase arsenic partitioning in sulfidic sediments. *Environ. Sci. Technol.* **36**, 4921-4927.

Wilkin R.T. and Ford R.G. (2006) Arsenic solid-phase partitioning in reducing sediments of a contaminated wetland. *Chem. Geol.* **228**, 156-174.

Wilkin, R.T., Wallschlager, D., and Ford, R.G. (2003) Speciation of arsenic in sulfidic waters. *Geochem Trans*. **4**, 1-7.

Zheng Y., Stute M., van Geen A., Gavrieli I., Dhar R., Simpson H J., Schlosser P.and Ahmed K.M. (2004) Redox control of arsenic mobilization in Bangladesh groundwater. *App. Geochem.* **19**, 201-214.

Table 1. Chemical composition of sediment from Rajoir and Srirampur. (Fe^{2+}_{HCl}, ferrous iron extracted by treatment of sediment with 0.5N HCl).

	Rajoir				Srirampur			
Element	Median	Minimum	Maximum	Number	Median	Minimum	Maximum	Number
As (ppm)	1.3	0.61	21	42	2.8	0.6	290	59
S (wt.%)	0.012	<0.005	0.17	38	0.027	<0.005	1.5	58
Corg (wt.%)	0.07	0.02	0.91	25	0.18	0.04	0.66	35
Fe^{2+}_{HCl} (wt.%)	0.37	0.08	1.7	36	0.66	0.13	6.3	43

Table 2. Abundance of arsenic-containing phases indicated by analyses of XANES spectra of bulk samples and individual grains.

Sample	Depth (m)	As (mg/kg)	Edge Position* (eV)	Fit Range (eV)	Percent of Model Compound (not normalized)**			energy shift (eV)	χ^2***
					Sulfide	*Arsenite Model*	*Arsenate Model*		
Srirampur borehole Ar-preserved sediment (bulk XANES)									
SH1-1	21.9	7	11869.1	60	22 As_2S_3	32 *(HAO)*	33 *(HAO)*	-0.8	16.7
SH1-9	83.2	10	11870.1	60	54 $Fe(As,S)_2$	44 *(HFO)*		-0.7	10.0
SH1-29	260.6	4	11869.2	60	73 $Fe(As,S)_2$	13 *(HAO)*	11 *(HAO)*	-1.6	4.5
SH1-36	326.1	74	11867.3	60	72 $Fe(As,S)_2$	9 *(siderite)*	19 *(HFO)*	0.2	0.3
SH1-39	355.1	6	11866.7	60	68 $Fe(As,S)_2$	15 *(siderite)*	16 *(HFO)*	-0.8	6.7
Rajoir borehole Ar-preserved sediment (bulk XANES)									
SH2-1	11.6	10	11869.1	60	81 $Fe(As,S)_2$		11 (*ferric phosphate, amorphous)*	-1.2	6.4
Rajoir Peat, surface pit	3	4	11869.5	60	48 As_2S_3	43 *(vivianite)*	14 *(vivianite)*	-0.09	2.6
Srirampur 39 m microXANES									
Area 1, spot1	39	n.d.	11866.6	90	113 $Fe(As,S)_2$			0.6	1.9
Area 1 spt2	39	n.d.	11866.4	90	102 $Fe(As,S)_2$			0.8	2.0
Area 1spot10	39	n.d.	11869.1	90		70 *(siderite)*	34 *(siderite)*	0.5	59.2
Area 1spot11	39	n.d.	11866.0	90	38 As_2S_3	56 *(vivianite)*	10 *(vivianite)*	0.9	1.7
Area 2 spot 1	39	n.d.	11866.4	90	98 $Fe(As,S)_2$		3 *(siderite)*	0.2	2.5
Area 2, Spot 2	39	n.d.	11865.7	50	87 $Fe(As,S)_2$		15 *(HFO)*	-0.2	4.0
Srirampur 326 m microXANES									
spot 1	326.1	n.d.	11865.7	250	99 $Fe(As,S)_2$			0.7	2.6
spot 2	326.1	n.d.	11866.1	250	100 $Fe(As,S)_2$			0.4	3.2
spot 6	326.1	n.d.	11866.2	250	100 $Fe(As,S)_2$			0.2	3.0
spot 3	326.1	n.d.	11866.2	250	90 $Fe(As,S)_2$		10 *(HFO)*	-0.5	2.0
spot 4	326.1	n.d.	11866.6	250	90 $Fe(As,S)_2$	3 *(siderite)*	7 *(siderite)*	-0.8	2.5
spot 5	326.1	n.d.	11866.3		76 $Fe(As,S)_2$	11 *(vivianite)*	20 *(vivianite)*	-0.3	2.8

* measured on the maximum of the 4 pt smoothed. 1st derivative of the XANES spectrum.
** HAO = hydrous aluminum oxide; HFO = hydrous ferric oxide. See text for details.
*** sum of squares of the residuals.

Table 3. Arsenic contents (ppm) of framboidal and massive morphologies from the depth intervals sampled. [min., minimum; max, maximum; n, number of analyses; np=not present]

			Framboid				Massive			
Locale	Sample	Depth (m)	min	max	median	n	min	max	median	n
Rajoir	SP41-1	2.5	<300	6020	2670	4	np	np	np	0
Rajoir	SH2-09	99	573	11030	4750	8	790	4640	2040	25
Rajoir	SH2-15	167	<300	6240	1210	24	300	11500	7230	14
Rajoir	SH2-37	450	350	8180	1600	5	320	12600	3570	14
Srirampur	SP-5-1	3.2	2700	9450	3570	6	np	np	np	0
Srirampur	SH1-01	22.6	<300	7360	1580	10	3600	6530	5750	4
Srirampur	SH1-12	114	<300	4220	1300	17	<300	6790	1270	5
Srirampur	SH1-37	355	577	6750	1930	7	470	5660	3810	7

List of figures:

Figure 1. Map of Bangladesh with location of study areas (↴) and major cities (✍).

Figure 2. Total arsenic, total sulfur, organic carbon (Corg), the content of silt and clay (<62 ?m), and the ratio of 0.5 N HCl extractable Fe^{2+}/Fe_{total} in sediment samples from Rajoir and Srirampur. Note the larger arsenic scale for the Srirampur borehole. Symbols on the right indicate samples analyzed using electron probe (☞), XAFS (↴) and sulfur speciation analyses (☞) of preserved samples. (↴ - sample from the unsaturated zone for determination of Fe^{2+}/Fe_{total}).

Figure 3. Mole ratio of arsenic to sulfur in bulk sediment samples. The shaded area corresponds to As:S ratios of most pyrite analyzed in this study. The maximum amount of arsenic measured in pyrite corresponds to a ratio of 0.009.

Figure 4. The concentration of arsenic sequentially extracted from preserved sediment samples collected from the Srirampur borehole. The extracts include 0.5 N HCl (exchangeable species, siderite and vivianite); Ti^{3+}-EDTA, (ferric oxides); and H_2O_2-HCl (sulfide phases).

Figure 5. Mineral sulfide abundance and isotope composition in sediment samples from Rajoir (✍) and Srirampur (✍). A) pyritic sulfur (PY), B) weight ratio of acid-volatile sulfide (AVS) and PY, C) $?^{34}S_{PY}$ of pyritic sulfur and D) the difference in the $?^{34}S$ composition of AVS and PY.

Figure 6. Energy position of model and bulk borehole XANES spectra. There is a shift of ~3 eV with each increase in nominal oxidation state. Selected models with well-defined oxidation states were used to generate the linear relationship between energy shift and nominal valence that was applied to sulfide model compounds and to samples.

Figure 7. MicroXAFS results of Srirampur sample (326.5 m). A) False color image illustrating grains with high arsenic and sulfur contents. B) Extended XANES spectra (solid lines) of spots 1, 3, and 4 and least-squares fits (dotted lines) show most arsenic is in pyrite. C) XANES spectrum of spot 5 (solid line), corresponding least squares fit (heavy dotted line) and fit deconvolution (lighter, labeled dotted lines). Note the similarity in the relative proportion of the arsenian pyrite peak to the

arsenate+arsenite peak in this microXANES spectrum to that of D) the bulk spectrum of the corresponding depth interval.

Figure 8. Backscattered electron images of pyrite forms in Bangladesh sediment. A) Open framboid texture (Rajoir 99 m). B) Massive overgrown framboid texture (Rajoir 167 m). C) Octahedral overgrowths on framboidal pyrite (Srirampur 355 m). D) Octahedral pyrite (Srirampur 355 m). Brighter zones indicate areas with greater arsenic contents. E) Massive pyrite formed by replacement of a biotite grain. Residual biotite was detected within the grain (Rajoir 450 m). F) Pyrite nucleating between biotite layers (Srirampur 1071 m).

Figure 9. Sulfur versus arsenic concentrations in pyrite measured by electron probe for Rajoir (bottom) and Srirampur (top) samples. The extent of arsenic substitution for sulfur is consistent with bulk sediment composition (Figure 3). (closed symbols=framboids; open symbols=massive).

Figure 10. Box plot comparing arsenic concentrations measured by EPMA between massive and (n=66) and framboidal pyrite (n=78) from both boreholes.

Figure 11. Probable depth intervals for the formation of framboidal (fram.) and massive pyrite based on petrographic observations. Concentration curves for sulfate and arsenic are best fit Loess lines calculated using the data of BGS and DPHE (2001). Plotted curves based on data from wells south of 23.5 north latitude and between 89.5 and 91.8 degrees east longitude (n = 907).

Figure 12. Generalized diagram of sulfur fluxes from natural sources into the subaerial sediment of the Bengal Basin. Fluxes estimated from the concentrations of sulfur as described in the electronic annex and assuming a 0.6 m a^{-1} annual recharge (BGS and DPHE, 2001). Influence of sea water likely is limited to within 100 km of the coastline. Contributions of river water are restricted to flood plains marginal to the rivers.

Electronic annex descriptive caption:

The electronic annex includes further details on x-ray absorption spectroscopy data reduction and fit procedures, a description of the sulfur supplies and fluxes to Bangladesh sediment, and data tables of sulfur abundance and isotopes and electron probe spot analyses of pyrite.

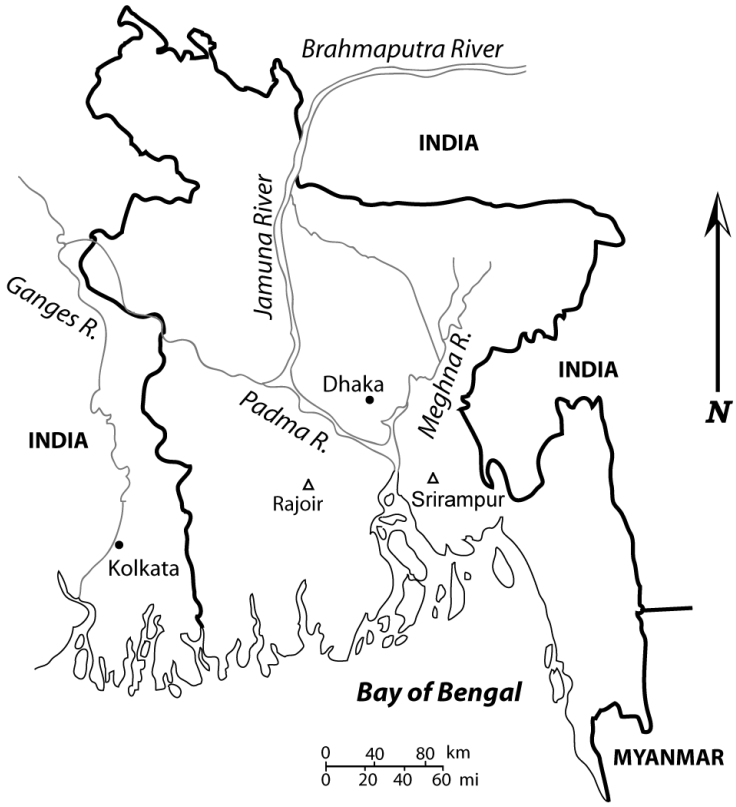

Fig.1

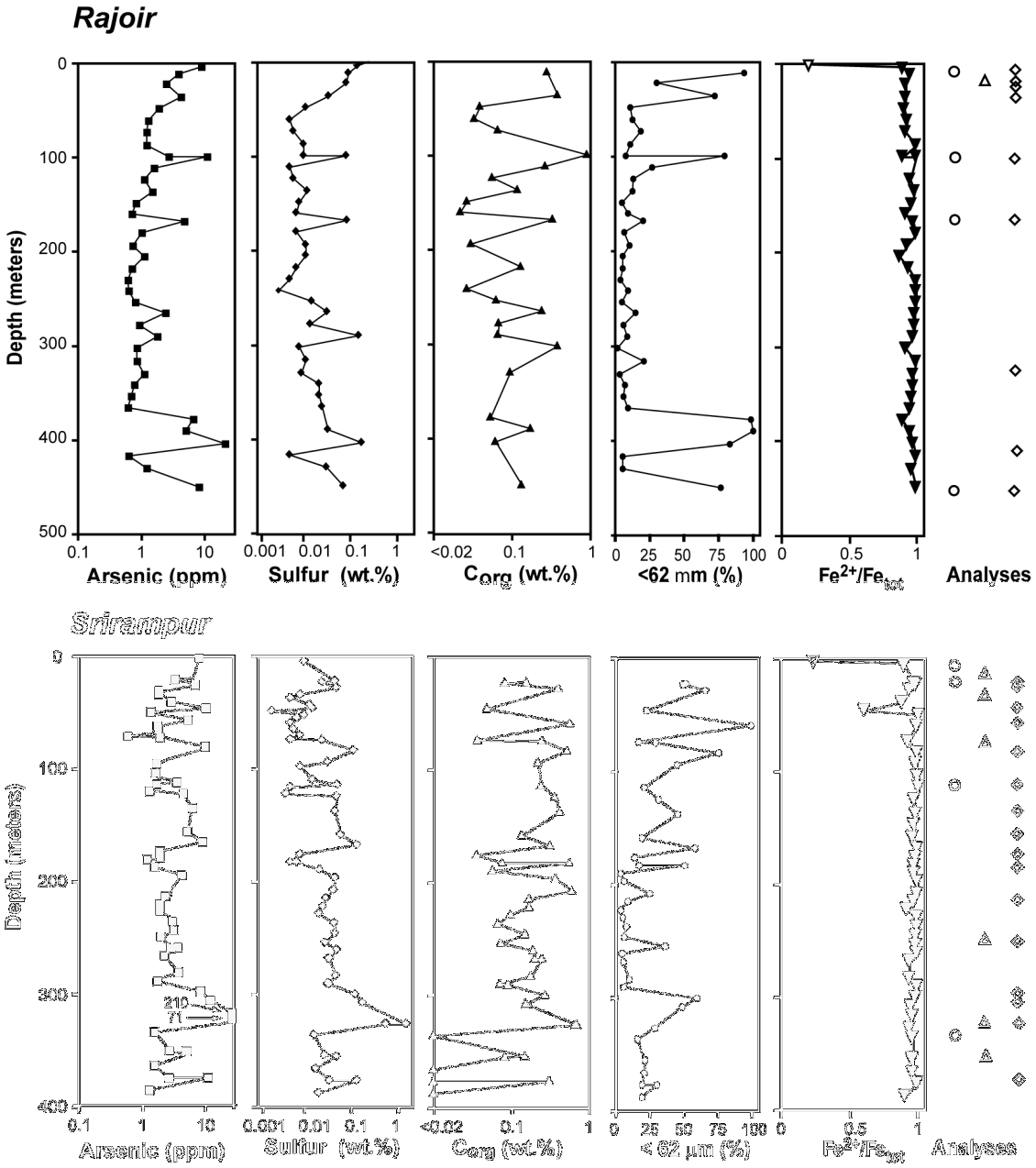

Fig.2

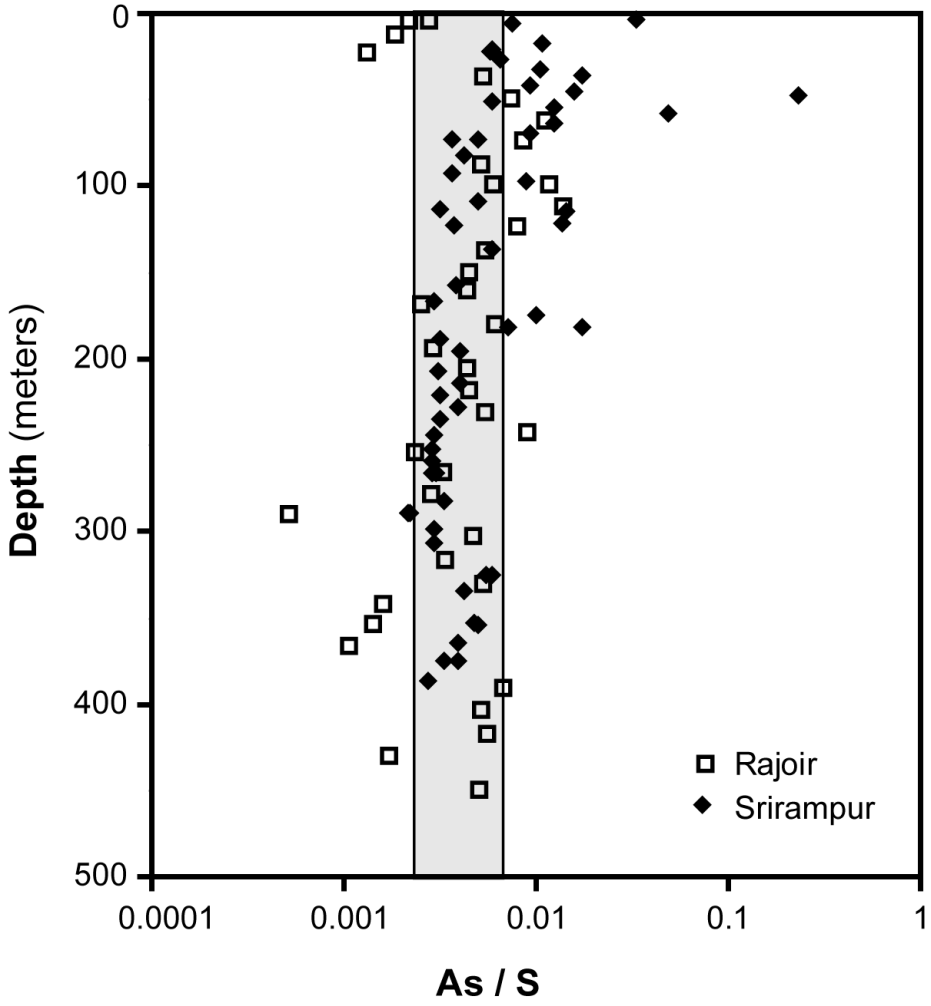

Fig.3

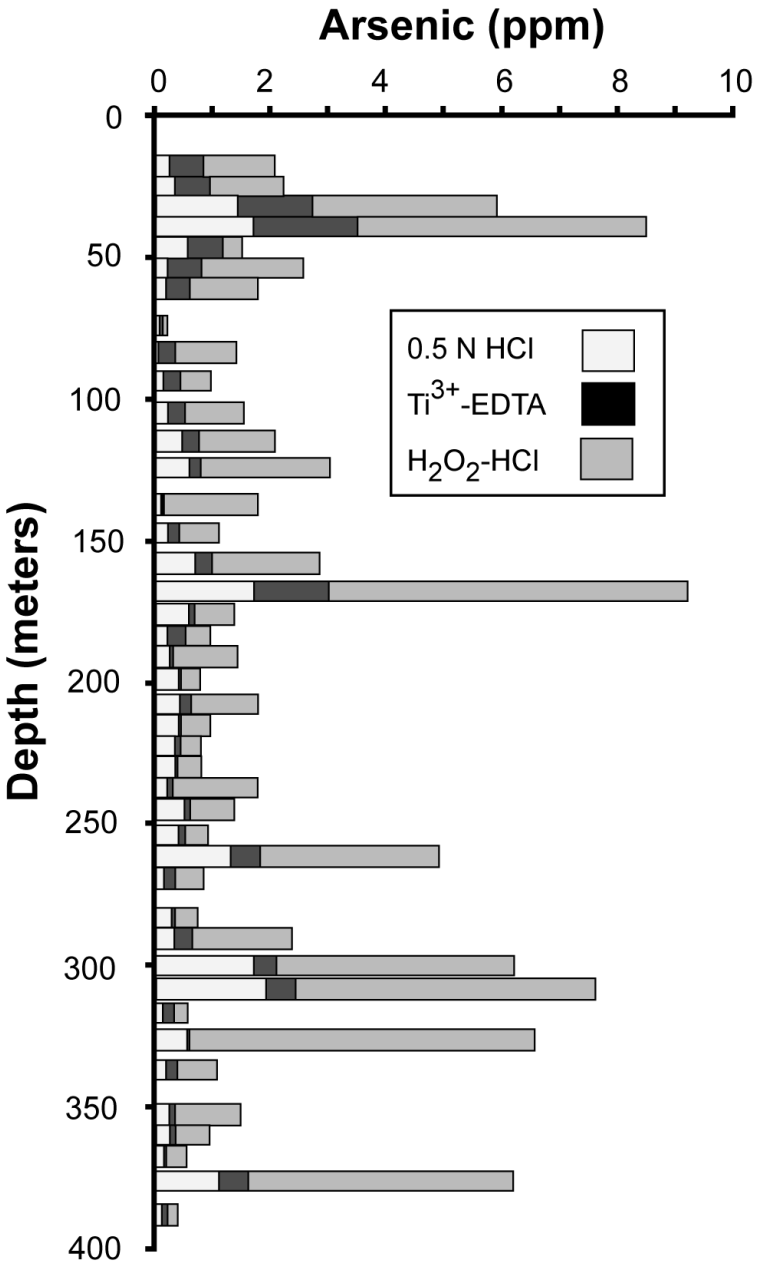

Fig.4

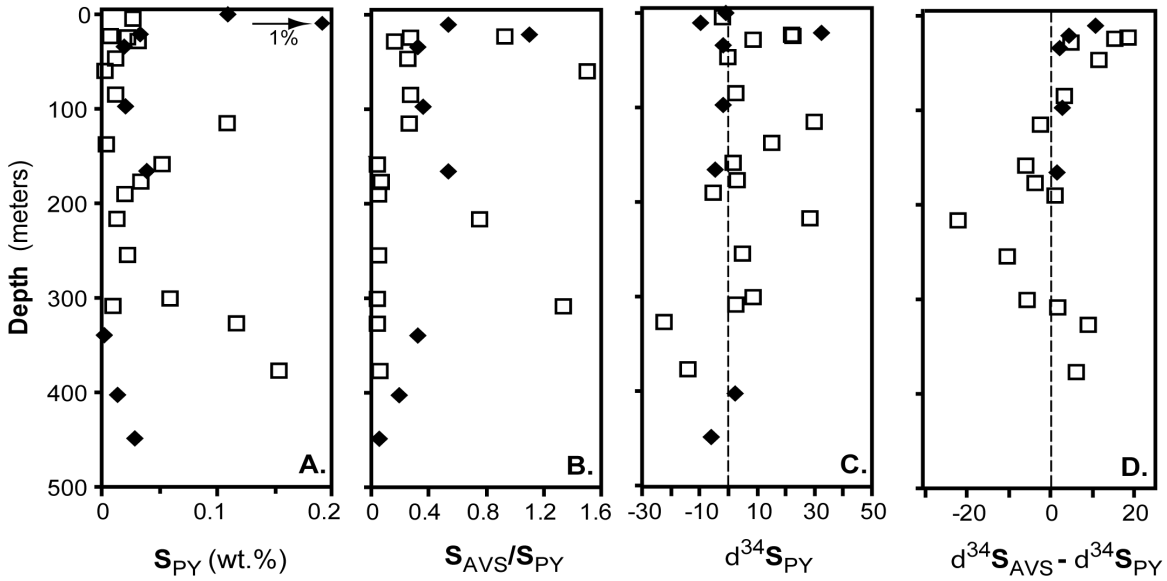
Depth (meters)
0
100
200
300
400
500
1%
A.
B.
C.
D.
0
0.1
0.2
0
0.4
0.8
1.2
1.6
-30
-10
10
30
50
-20
0
20
S_{PY} (wt.%)
S_{AVS}/S_{PY}
$d^{34}S_{PY}$
$d^{34}S_{AVS}$ - $d^{34}S_{PY}$

Fig.5

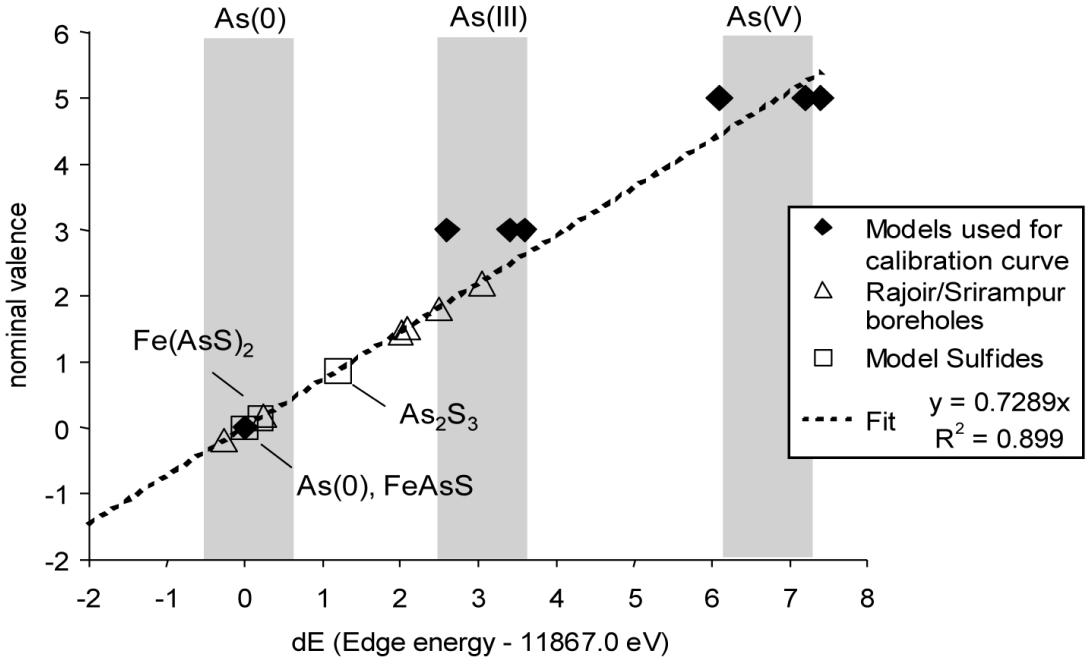
As(0)
As(III)
As(V)
nominal valence
6
5
4
3
2
1
0
-1
-2
-2
-1
0
1
2
3
4
5
6
7
8
dE (Edge energy - 11867.0 eV)
Fe(AsS)2
As2S3
As(0), FeAsS
Models used for calibration curve
Rajoir/Srirampur boreholes
Model Sulfides
Fit
y = 0.7289x
R2 = 0.899

Fig.6

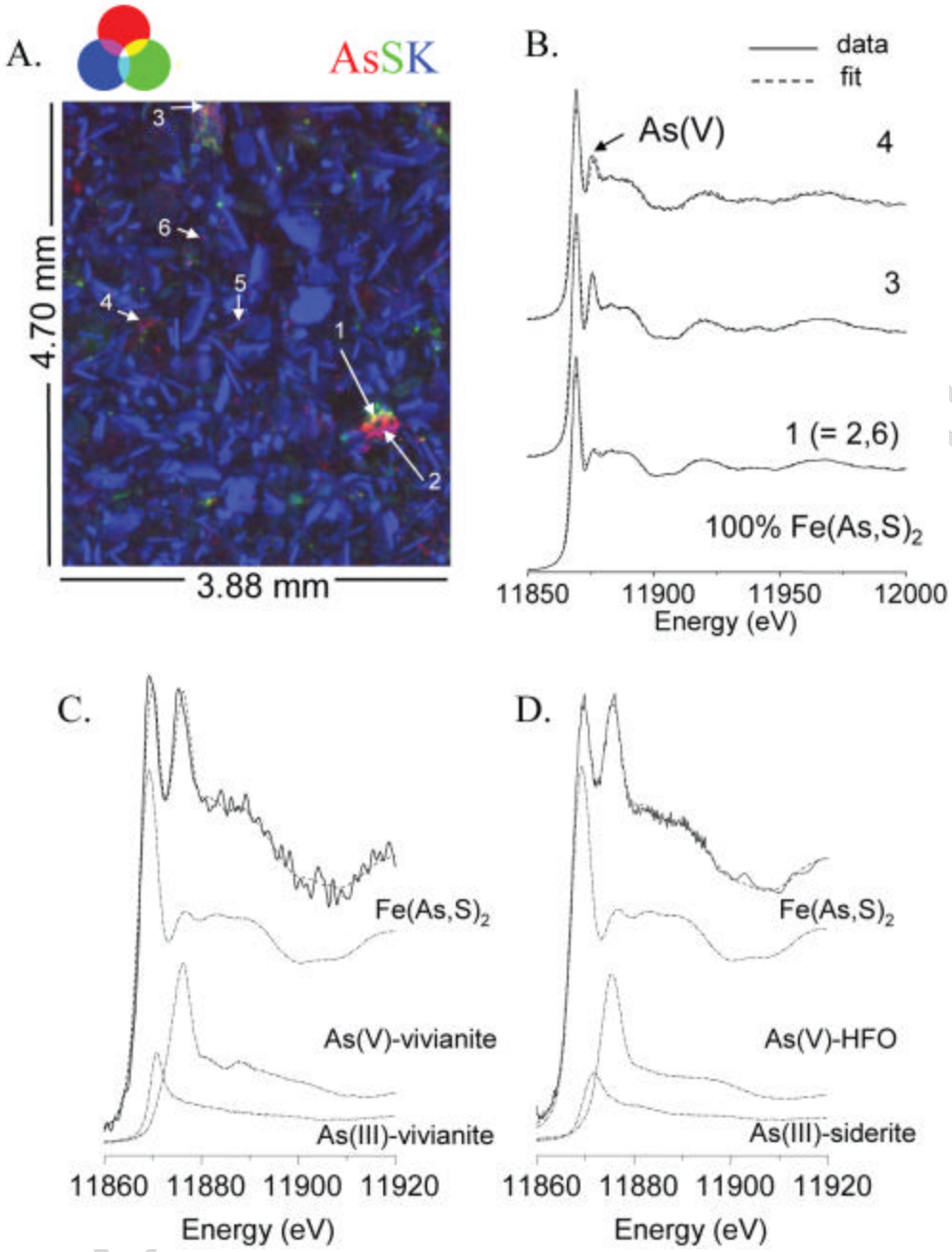
A.
AsSK
3
6
5
4
1
2
4.70 mm
3.88 mm
B.
data
fit
As(V)
4
3
1 (= 2,6)
100% Fe(As,S)2
11850
11900
11950
12000
Energy (eV)
C.
Fe(As,S)2
As(V)-vivianite
As(III)-vivianite
11860
11880
11900
11920
Energy (eV)
D.
Fe(As,S)2
As(V)-HFO
As(III)-siderite
11860
11880
11900
11920
Energy (eV)

Fig.7

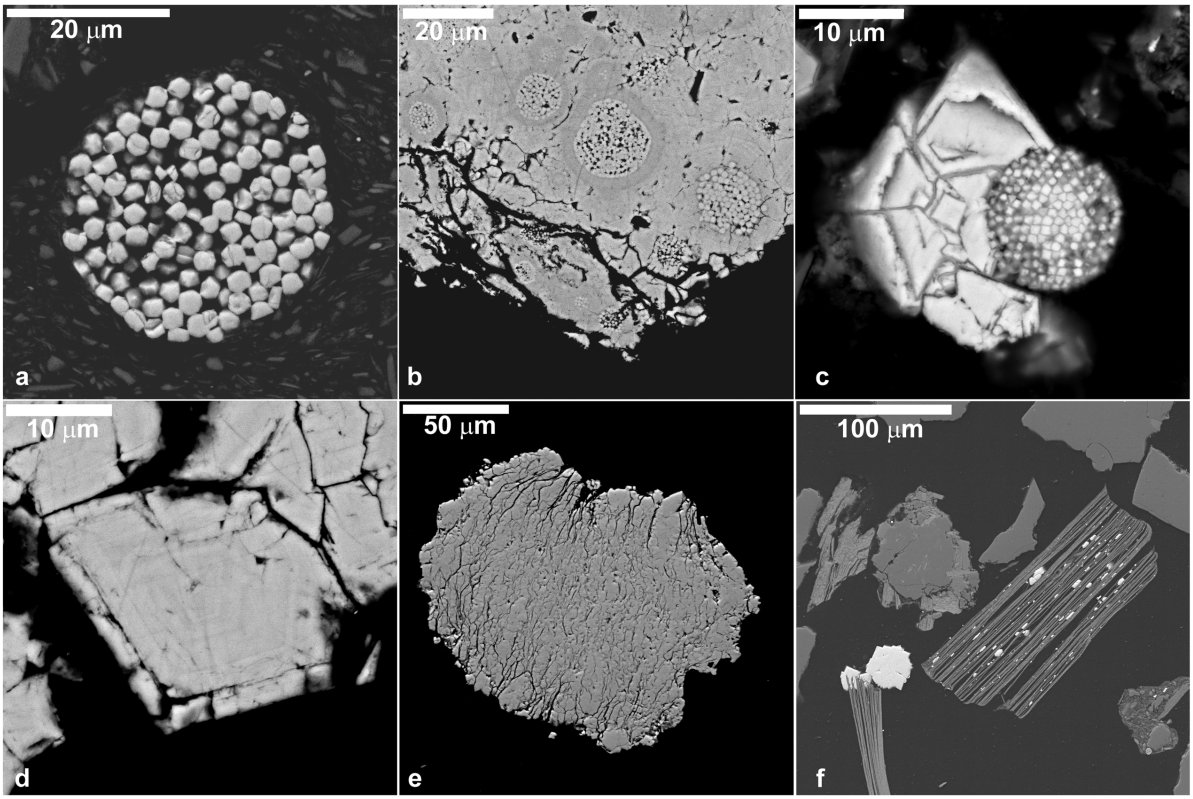

Fig.8

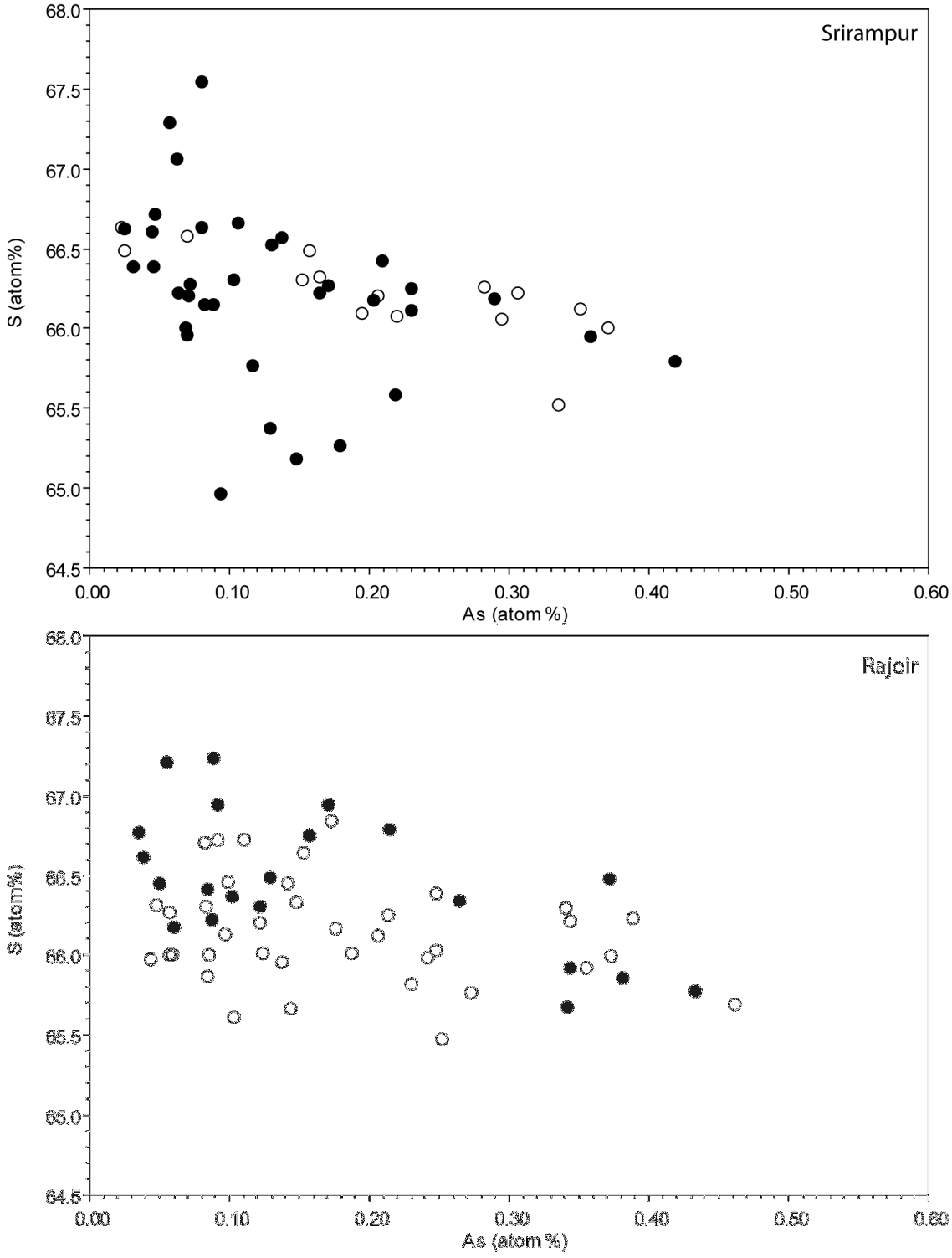

Fig.9

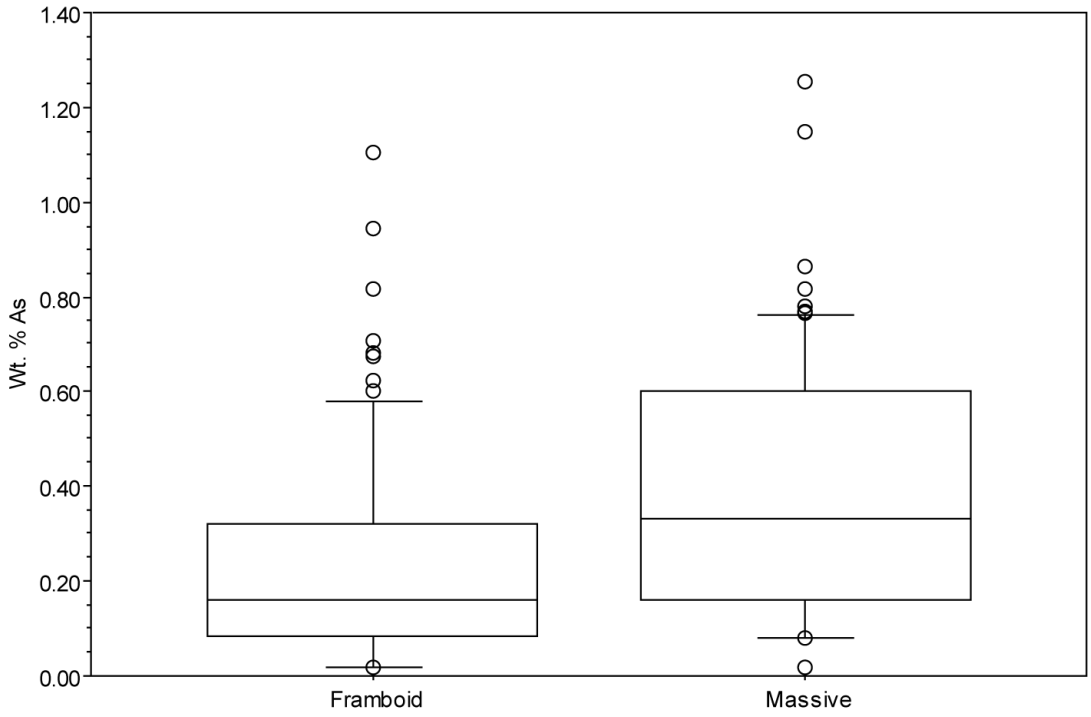

Fig.10

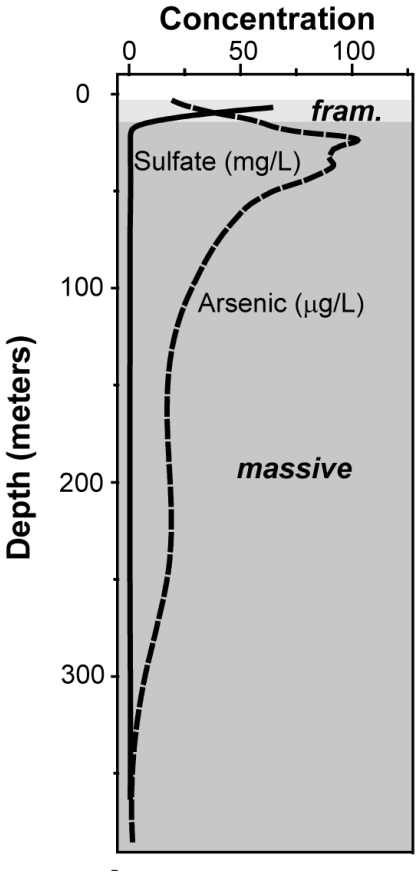
Concentration
0
50
100
0
100
200
300
Depth (meters)
fram.
Sulfate (mg/L)
Arsenic (μg/L)
massive

Fig.11

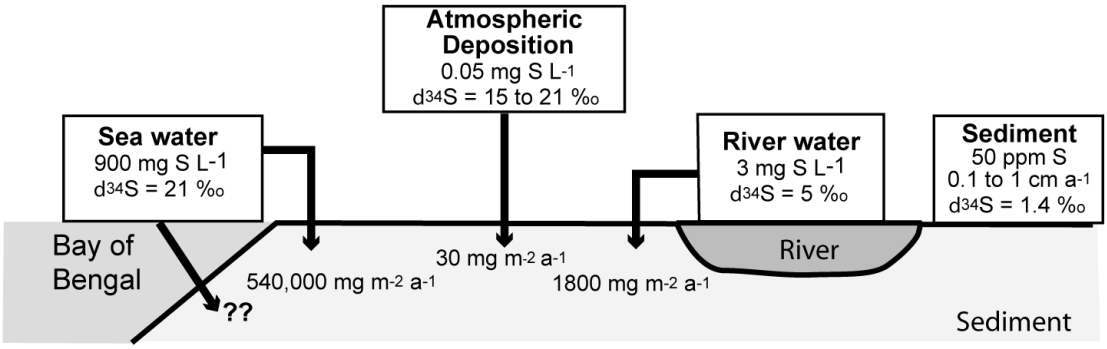
Atmospheric Deposition
0.05 mg S L-1
d34S = 15 to 21 ‰
Sea water
900 mg S L-1
d34S = 21 ‰
River water
3 mg S L-1
d34S = 5 ‰
Sediment
50 ppm S
0.1 to 1 cm a-1
d34S = 1.4 ‰
Bay of Bengal
??
540,000 mg m-2 a-1
30 mg m-2 a-1
1800 mg m-2 a-1
River
Sediment

Fig.12

Electronic Annex: Arsenic incorporation into authigenic pyrite, Bengal Basin sediment, Bangladesh

Heather A. Lowers[a,*], George N. Breit[a], Andrea L. Foster[b], John Whitney[c], James Yount[c], Md. Nehal Uddin[d] and Ad. Atual Muneem[d]

[a]*U.S. Geological Survey, MS 973, Denver, Colorado, U.S.A*
[b]*U.S. Geological Survey, MS 901, Menlo Park, California, U.S.A*
[c]*U.S. Geological Survey, MS 980, Denver, Colorado, U.S.A*
[d]*Geological Survey of Bangladesh, Segenbagicha, Dhaka, Bangladesh*

Appendix 1: XAFS Data Analysis Procedures

Native arsenic, compounds containing arsenate oxyanion, and compounds containing the arsenite oxyanion have well-defined nominal valences and substantial energy shifts that can readily be discriminated by XANES analysis; several of these compounds were used to construct a calibration curve relating valence to edge energy shift relative to that of native arsenic (assigned a value of zero; Figs. 6 and EA-1). XANES spectra of arsenic in sulfide model minerals were not used to construct the calibration curve, because the nominal valence arsenic in many of these minerals is not well known (Foster, 2003). The estimated valences of arsenic in arsenopyrite, arsenian pyrite, and orpiment as derived from this calibration curve are 0, +0.1, and +0.9, respectively.

The procedure for fitting bulk and micro-XANES spectra collected from sediment samples was as follows: the energy position of the arsenic model compound spectra used in fits were fixed, and that of the sample spectrum allowed to vary. Often a two-component fit with very small shifts in sample energy position (average of - 0.1 eV shift, n = 26) was sufficient to match the features of the XANES spectrum. For samples in which two components were insufficient, additional models were considered one-by-one until χ^2 was minimized. Thirteen XANES spectra were tested in fits: (1) native As, (2) arsenopyrite (FeAsS), (3) arsenian pyrite [$Fe(As,S)_2$], (4) orpiment (As_2S_3); arsenite co-precipitated in HAO (5), co-precipitated in siderite (6), adsorbed to vivianite (7) and adsorbed to HFO (8); arsenate co-precipitated in HAO (9), co-precipitated in

siderite (10), co-precipitated in amorphous ferric phosphate (11), adsorbed to HFO (12), and in scorodite ($FeAsO_4 \cdot 2H_2O$) (13).

Discrimination among various forms of arsenic-bearing sulfides is central to the work reported here, so it should be noted that although the shifts in energy position are small between the arsenic-bearing sulfides examined (and therefore are unreliable indicators of arsenic residence in a particular sulfide), there are substantial differences between the XANES and EXAFS spectral lineshapes (as well as difference in the size and position of features in the Fourier transforms) of the three arsenic sulfides examined as a part of this study (Fig. EA-1; the distance scale in the Fourier transform has not been corrected for phase shift, so measured distances are therefore approximately 0.5 Å shorter than true distances). These differences indicate that the number and distance of atoms surrounding arsenic is substantially different in each of the three phases, as has been discussed at length elsewhere (Foster et al., 1998b; Savage et al., 2000; O'Day et al., 2004).

Appendix 2: Sulfur supply

The natural sulfur sources to the Bengal Basin sediment include atmospheric deposition, proximal weathering of detrital sulfides, riverine input and sea water. To evaluate the contribution of sulfur from these sources we assumed: 1) all sulfate entering the subsurface is converted to sulfide sulfur within 20 m of the ground surface, 2) sediment accumulation rates varied between 0.1 and 1 cm a^{-1} (Goodbred and Kuehl, 2000), and 3) recharge was limited to the equivalent of 0.6 m a^{-1} (BGS and DPHE, 2001).

Atmospheric deposition

The modern atmospheric flux of sulfur is estimated to be 100 mg m^{-2} a^{-1}, mainly through wet deposition (Robertson et al., 1995). Considering a median annual rainfall of 2 m a^{-1} in the vicinity of the boreholes (BGS and DPHE, 2001) and infiltration of 0.6 m a^{-1} (BGS DPHE, 2001) the resulting atmospheric deposition contributes 30 mg S m^{-2} a^{-1}. Using sulfur isotopes, Jacks et al., (1994) verified that sea water is the principal source of sulfur in monsoon precipitation on the Indian subcontinent and this sulfur likely has an isotopic composition ranging from +15 to +21 per mil (Krouse and Mayer, 2000).

Detrital Sulfides

Low concentrations of sulfur in river sand and sediment above the saturated zone (<0.005 wt.% S) indicate that proximal oxidation of detrital sulfide, although present as trace microscopic grains, is a small source of sulfate. The low sulfur content of surficial sediment supports oxidative loss during weathering proposed by Polizzotto et al. (2005), however, this loss may have been largely complete prior to deposition (Ravenscroft et al., 2005). If sulfide sulfur were present at 50% of the analytical detection limit, the amount of sulfur deposited on the sediment surface at a 1 cm a^{-1} deposition rate would be 390 mg S m^{-2} a^{-1}. The $?^{34}S$ of detrital sulfide (1.4

per mil) is based on the composition of detrital pyrite collected from the Narayani River, Nepal north of the town of Narayanghat near the last outcrop of crystalline rocks along the drainage.

River Water

Rivers transport four million tons of dissolved sulfur annually through the Bengal basin at concentrations of approximately 3 mg S L^{-1} (Datta and Subramanian, 1997). This sulfur is added to deposited sediment through infiltration of floodwater and as a result of bank infiltration during high river levels (BGS and DPHE, 2001). Infiltration of river water would result in a flux of 1800 mg S m^{-2} a^{-1} in those areas affected by overbank flooding. The measured isotope composition of dissolved sulfate in the Meghna River of 5 per mil is consistent with riverine sulfur derived from weathering of pyrite in the Himalayas and atmospheric deposition (Galy and France-Lanard, 1999).

Sea water

Sea water contains large concentrations of sulfate sulfur (900 mg L^{-1}) but its exposure to the terrestrially deposited Bengal basin sediment is temporally and spatially variable. During the dry season (November-April), saline water from the ocean penetrates surface drainages as far as 100 km inland (Allison, 1998). Infiltration of this saline water into the sediment may account for greater salinity of ground water along the margins of the Padma and lower Meghna river channels (Ravenscroft, 2003). Inundation by storm surges is also recognized as far as 100 km inland (Allison, 1998) resulting in salinization of wells and soils (Ravenscroft and McArthur, 2004; Sarma, 1996). Brackish water in the subsurface several hundred kilometers inland is also attributed to sea water (Ravenscroft and McArthur, 2004). Sea water intrusion into aquifers may also affect coastal sediments but the landward extent of this process is uncertain. Modern sea water sulfate has a $?^{34}S$ of 21 per mil.

Anthropogenic modifications

Although not relevant to the ancient record of sulfide mineral formation, the modification of sulfur fluxes by human activities will be significant in evaluating the future importance of sulfide formation. Sulfur supplied to modern sediment is affected by: a) the application of fertilizer to offset depletion of sulfur in agricultural soils (123,000 tons S in 1999; Bangladesh Agricultural Research Council), b) levees and channels have been constructed to reduce the extent of uncontrolled river flooding and supply irrigation water kilometers from the current river channels and c) the increasing density of population which is considered responsible for increased sulfate concentrations in ground water near villages (Burgess et al., 2002).

References

Burgess W.G., Burren M., Perrin J. and Ahmed K.M. (2002). Constraints on the sustainable development of arsenic-bearing aquifers in southern Bangladesh. Part 1: A conceptual model of arsenic in the aquifer. IN: Hiscock K.M., Rivett M.O., and Davison R.M., (Eds.) Sustainable groundwater development. Geological Society, London, Special Publication **193,** 145-163.

Datta D.K. and Subramanian V. (1997) Nature of solute loads in the rivers of the Bengal drainage basin, Bangladesh. *J. of Hydrology* **198**, 196-208.

Foster A.L. (2003) Spectroscopic investigations of arsenic species in solid phases. In: Welch A.H. and Stollenwerk K.G. (Eds.), Arsenic in Groundwater: Geochemistry and Occurrence. Kluwer Academic Publishers, Norwell, 475 p.

Jacks G., Sharma V.P., Torssander P. and Aberg G. (1994) Origin of sulphur in soil and water in a Precambrian terrain, S. India. *Geochem J*, **28**, 351-358.

Krouse H.R. and Mayer Bernard (2000) Sulfur and oxygen isotopes in sulphate, In, Cook P.L. and Herczeg A.L., (Eds), Environmental Tracers in Subsurface Hydrology, Kluwer, Boston, 195-231.

Robertson L., Rodhe H.and Grannat L. (1995) Modeling of sulfur deposition in the southern Asian region. *Water Air and Soil Poll*. **86**, 2337-2343.

Rowland H.A.L, Polya D.A., Lloyd, J.R., and Pancost R.D. (2006) Chracterisation of organic matter in a shallow, reducing, arsenic-rich aquifer, West Bengal. *Org. Geochem.* **37**, 1004-1114.

Sarma A.K.S. (1996) Reconstructing the great Bengal cyclone of 1737. *Mausam* **47**, 67-72.

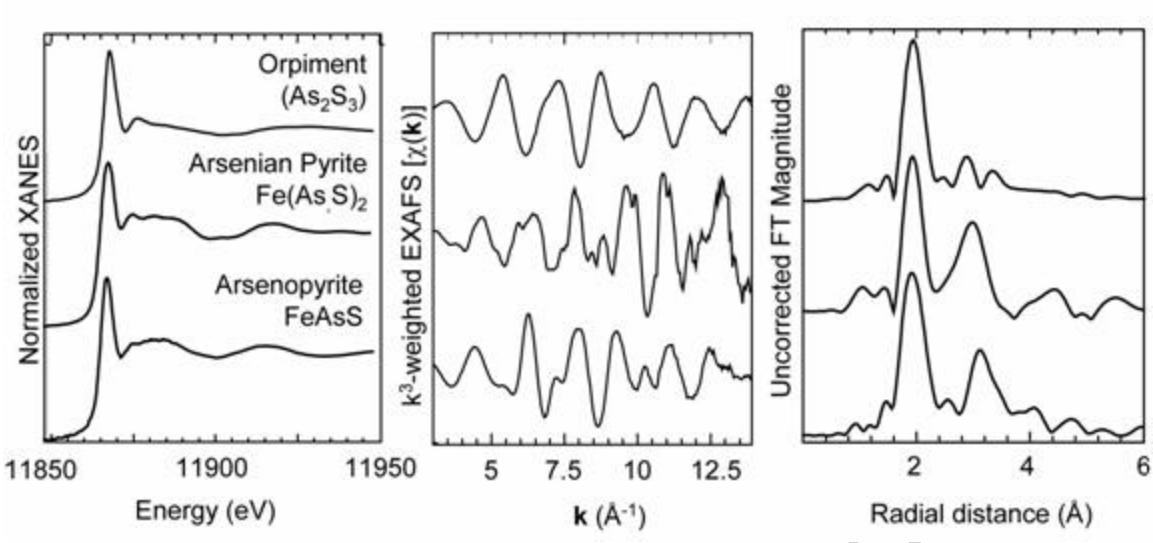

Figure EA-1. Distinct differences in the XANES spectra, the EXAFS spectra, and the Fourier transform (FT) of the EXAFS spectra indicate substantial differences in the number, identity, and distance of atoms within 6 Å of the average arsenic atom in these materials; this information was used to identify sulfide-associated arsenic in borehole sediments.

Table EA-1. Concentration and isotopic composition of acid-volatile sulfide (AVS), pyritic sulfur (DI), and sulfate (SO_4) extracted from sediment samples and reference sources of sulfur. Composite ?^{34}S is the weighted average of AVS and DI sulfide. [nd=not determined; na, not applicable]

Sample	Location	Depth (m)	Sulfide$_{(AVS)}$ (ppm)	Sulfide$_{(DI)}$ (ppm)	Acid-soluble$_{(SO4)}$ (ppm)	?$^{34}S_{AVS}$ (per mil)	?$^{34}S_{DI}$ (per mil)	?$^{34}S_{SO4}$ (per mil)	Composite?? ?$^{34}S_{sulfide}$
SP-36 2.2	Rajoir	2.2	nd	100	nd	nd	-1.4	nd	-1.4
SP-41 1	Rajoir	2	nd	1110	nd	nd	-0.4	nd	-0.4
SH-2 1	Rajoir	11.6	5250	9580	100	1.9	-9.1	35.3	-5.2
SH-2 2	Rajoir	22	390	350	50	37.7	32.9	nd	35.4
SH-2 3	Rajoir	35.7	70	210	130	1.2	-1.3	nd	-0.7
SH-2 9	Rajoir	98.9	80	214	60	2.1	-1.1	nd	-0.2
SH-2 15	Rajoir	167.7	220	400	50	-2.3	-4.1	nd	-3.5
SH-2 29	Rajoir	341.5	10	30	50	nd	nd	nd	nd
SH-2 34	Rajoir	403.4	30	150	50	nd	2.8	nd	2.3
SH-2 37	Rajoir	449.7	20	300	30	nd	-5.6	nd	-5.3
SP-5 1	Srirampur	4	nd	270	nd	nd	-2.3	nd	-2.3
SH-1 1	Srirampur	22.6	65	70	10	39.9	21.6	nd	30.4
SH-1 2	Srirampur	23.3	60	220	10	37.4	22.4	nd	25.6
SH-1 3	Srirampur	27.4	50	310	<10	13.1	8.6	nd	9.2
SH-1 5	Srirampur	46.5	30	120	<10	10.7	-0.5	nd	1.7
SH-1 7	Srirampur	59.8	30	20	<10	3.7	nd	nd	2.2
SH-1 9	Srirampur	83.8	30	110	10	5.7	2.6	nd	3.3
SH-1 12	Srirampur	114.5	280	1090	80	27.0	29.8	22.4	29.2
SH-1 14	Srirampur	137.5	nd	38	nd	nd	14.7	nd	14.7
SH-1 16	Srirampur	158.5	20	520	<10	-4.6	1.5	nd	1.2
SH-1 18	Srirampur	176.1	20	330	<10	-1.1	2.7	nd	2.5
SH-1 20	Srirampur	189.9	10	200	<10	-4.7	-5.5	nd	-5.5
SH-1 23	Srirampur	215.5	96	128	nd	3.7	26.1	nd	16.5
SH-1 28	Srirampur	253.8	10	220	40	-6.1	4.6	26.1	4.1
SH-1 33	Srirampur	300.1	20	590	110	2.6	8.3	14.1	8.2
SH-1 34	Srirampur	307.8	120	90	15	3.7	2.3	35.3	3.1
SH-1 36	Srirampur	326.5	40	1170	70	-13.8	-22.7	-13.5	-22.4
SH-1 41	Srirampur	376.2	80	1540	<10	-8.4	-14.2	nd	-13.9
Meghna River Water	Bhairab	0	na	na	6.1 (mg/L)	na	na	4.8	na
Barite	drilling mud	na	na	na	na	na	na	19.4	na
Fertilizer	Gypsum, NH_4SO_4, $MgSO_4$, NPKS	na	na	na	na	na	na	15.3, 4.8, 13, 14.8	na

Table EA-2. Electron probe analyses of selected pyrite from Srirampur and Rajoir. Cu and Zn were below detection (< 100 ppm) in all authigenic pyrite morphologies. Analyses which had high Si and (or) Mg were not used due to possible interference from surrounding phases.

Locale	Sample	Fe (wt%)	As (wt%)	S (wt%)	Total	Fe (atom%)	As (atom %)	S (atom%)	Morphology	Size (um)	Depth (m)
Rajoir	SP41-1	44.6	0.60	52.5	97.7	32.67	0.33	67.00	framboid-filled	17	3
Rajoir	SP41-1	44.4	0.16	52.5	97.0	32.68	0.09	67.23	framboid-filled	25	3
Rajoir	SH2-09	47.1	0.06	52.3	99.4	33.95	0.03	65.73	framboid-filled	27	99
Rajoir	SH2-09	46.2	0.16	52.8	99.2	33.35	0.08	66.41	framboid-open	33	99
Rajoir	SH2-09	46.6	0.71	52.2	99.4	33.76	0.38	65.86	framboid-open	14	99
Rajoir	SH2-09	47.1	0.27	51.8	99.2	34.13	0.15	65.45	massive-anhedral	5	99
Rajoir	SH2-09	46.8	0.45	52.9	100.1	33.51	0.24	65.99	massive-anhedral	8	99
Rajoir	SH2-09	46.4	0.17	53.5	100.1	33.19	0.09	66.72	massive-cube	6	99
Rajoir	SH2-09	46.3	0.40	52.6	99.3	33.54	0.21	66.25	massive-octahedron	5	99
Rajoir	SH2-09	47.2	0.11	52.7	100.1	33.94	0.06	66.00	massive-octahedron	5	99
Rajoir	SH2-15	46.7	bdl	53.0	99.6	33.51	---	66.27	framboid-filled	29	167
Rajoir	SH2-15	46.4	0.30	53.8	100.5	33.09	0.16	66.75	framboid-filled	17	167
Rajoir	SH2-15	45.9	0.03	52.2	98.1	33.40	0.02	66.17	framboid-open	27	167
Rajoir	SH2-15	46.5	bdl	53.1	99.6	33.34	---	66.25	framboid-open	14	167
Rajoir	SH2-15	45.4	1.15	51.8	98.3	33.21	0.63	65.99	massive-anhedral	13	167
Rajoir	SH2-15	46.3	0.03	52.9	99.2	33.32	0.02	66.37	massive-anhedral	11	167
Rajoir	SH2-15	46.3	0.64	52.9	99.9	33.32	0.34	66.29	massive-cube	6	167
Rajoir	SH2-37	46.8	0.11	52.7	99.6	33.76	0.06	66.18	framboid-filled	17	450
Rajoir	SH2-37	47.1	0.82	53.1	101.0	33.52	0.43	65.77	framboid-filled	10	450
Rajoir	SH2-37	46.5	0.66	52.2	99.4	33.72	0.36	65.92	massive-anhedral	30	450
Rajoir	SH2-37	47.3	0.03	53.0	100.4	33.85	0.02	66.13	massive-anhedral	20	450
Srirampur	SP-5-1	46.4	0.39	53.0	99.9	33.37	0.21	66.43	framboid-open	9	3
Srirampur	SP-5-1	47.1	0.32	53.4	100.8	33.56	0.17	66.27	framboid-open	37	3
Srirampur	SH1-01	46.0	0.13	52.3	98.4	33.44	0.07	66.20	framboid-filled	12	23
Srirampur	SH1-01	47.1	0.13	52.7	99.9	33.83	0.07	66.01	framboid-open	10	23
Srirampur	SH1-01	46.3	0.65	52.6	99.6	33.45	0.35	66.12	massive-anhedral	7	23
Srirampur	SH1-01	44.9	0.36	52.4	97.7	32.52	0.19	66.10	massive-octahedron	3	23
Srirampur	SH1-12	46.5	0.19	53.2	100.0	33.26	0.10	66.30	framboid-filled	8	114

Locale	Sample	Fe (wt%)	As (wt%)	S (wt%)	Total	Fe (atom%)	As (atom %)	S (atom%)	Morphology	Size (um)	Depth (m)
Srirampur	SH1-12	46.3	0.31	52.5	99.1	33.48	0.16	66.22	framboid-filled	14	114
Srirampur	SH1-12	46.7	bdl	53.3	100.1	33.38	---	66.37	framboid-filled	8	114
Srirampur	SH1-12	45.3	0.05	52.5	97.9	33.00	0.03	66.63	framboid-open	8	114
Srirampur	SH1-12	46.0	0.38	52.3	98.6	33.37	0.20	66.18	framboid-open	11	114
Srirampur	SH1-12	45.6	0.28	52.4	98.3	33.18	0.15	66.30	massive-anhedral	10	114
Srirampur	SH1-12	46.1	0.04	52.9	99.0	33.29	0.02	66.63	massive-anhedral	7	114
Srirampur	SH1-37	46.6	0.09	52.9	99.6	33.57	0.05	66.39	framboid-filled	10	355
Srirampur	SH1-37	47.4	0.68	53.2	101.3	33.69	0.36	65.95	framboid-filled	10	355
Srirampur	SH1-37	45.2	0.53	51.3	97.0	33.53	0.29	66.18	framboid-open	10	355
Srirampur	SH1-37	46.1	0.57	52.4	99.1	33.47	0.31	66.22	massive-anhedral	20	355
Srirampur	SH1-37	46.6	0.31	52.9	99.8	33.51	0.16	66.32	massive-anhedral	10	355
Srirampur	SH1-37	46.8	0.05	53.3	100.2	33.49	0.03	66.48	massive-octahedron	30	355